Primordial black hole formation in k-inflation models

Neven Bilić[*]

*Division of Theoretical Physics, Rudjer Bošković Institute,
Zagreb, Croatia*

Dragoljub D. Dimitrijević[†], Goran S. Djordjević[‡], Milan Milošević[§]
Department of Physics, University of Niš, Serbia

Marko Stojanović[¶]
Faculty of Medicine, University of Niš, Serbia

December 22, 2025

Abstract

The local primordial density fluctuations caused by quantum vacuum fluctuations during inflation grow into stars and galaxies in the late universe and, if they are large enough, also produce primordial black holes. We study the formation of the primordial black holes in k-essence inflation models with a potential characterized by an inflection point. The background and perturbation equations are integrated numerically for two specific models. Using the critical collapse and peaks formalism, we calculate the abundance of primordial black holes today.

1   Introduction

According to the original idea of Zel'dovich and Novikov [1], highly overdense regions of inhomogeneities in the early universe could gravitationally collapse to form black holes (BHs) [2, 3, 4, 5], the so-called primordial black holes (PBHs) [5, 6]. It has been argued that PBHs may represent a non-negligible component of cold dark matter that provides the seed for the supermassive BHs that populate the universe.

To generate sufficiently large primordial fluctuations during inflation and form superdense regions that can collapse and become PBHs during the radiation-dominated era, the inflationary scalar perturbations need to be amplified by several orders of magnitude on small scales, i.e.,

---

[*]bilic@irb.hr, corresponding author

[†]ddrag@pmf.ni.ac.rs

[‡]gorandj@junis.ni.ac.rs

[§]milan.milosevic@pmf.edu.rs

[¶]marko.stojanovic@pmf.edu.rs

for wavenumbers q that are large compared with the pivot scale q_{CMB} of the cosmic microwave background (CMB). These scales correspond to the late stages of inflation and are well above the values required to be consistent with CMB observations.

An overdense region collapses and forms a PBH when the local value of the density contrast $\delta = \delta\rho/\rho$ is above the so-called collapse threshold density contrast δ_c. With the help of Newton's gravity and Jeans' radius $R_J \sim c_s/H$, it was established that PBH forms when the density contrast at the entry of a certain comoving scale q into the acoustic horizon (i.e., when $c_s q = aH$) exceeds a threshold value $\delta_c \sim c_s^2$ [7]. Here, c_s is the speed of sound equal to $1/\sqrt{3}$ in the case of radiation dominance. The mass of the resulting PBH is approximately equal to the mass within the horizon at the time of formation. Numerical checks for different primordial perturbation profiles show that during radiation dominance, the value for the threshold density contrast δ_c is in the range from 0.4 to 2/3 [8, 9, 10].

Depending on the mass, PBHs trigger different observational signals. PBHs lighter than $\sim 10^{15}$ g are already evaporated today by Hawking radiation and do not exist in today's Universe. Nevertheless, they leave some traces that allow us to investigate how many PBHs might have existed in the early Universe. The abundance of PBHs lighter than 10^{15} g, for example, is constrained by the Big Bang nucleosynthesis since the evaporation of high-energy particles changes the abundance of light elements [11].

PBHs heavier than 10^{15} g have not yet lost their mass significantly by evaporation and remain in the present Universe. They produce various distinct signals at present time, such as

- gravitational lensing,

- dynamical effects on baryonic matter,

- radiation emanating from the accreting matter into PBHs.

The choice of the physical process needed to show the existence of PBHs depends on the BH mass [12, 13, 14, 15, 16, 17]. For instance, gravitational lensing of background stars is the most powerful method to search for sub-solar PBHs. Accretion and dynamical effects on baryonic matter become more important for heavier PBHs.

There are various scenarios for primordial black hole production, such as: formation of PBHs during the reheating phase at the end of inflation [18], inflaton potential with inflection [9, 19, 20, 21, 22, 23, 24, 25], sound speed resonace during inflation [26, 27], null-energy condition violation during inflation [28], first order phase transitions [29], and inflation models with non-canonical kinetic terms [30, 31].

We aim to investigate PBH production in the early Universe in two inflation models both with a potential with inflection and noncanonical kinetic terms, in particular the Dirac-Born-Infeld (DBI) type of Lagrangian. The models in which the kinetic term has a noncanonical form are usually referred to as k-essence [32] or, in the context of inflation, k-inflation models [33]. In this work, we study two k-essence models using the Hamiltonian formalism for the background field equations.

First, we investigate a k-essence model proposed by Papanikolaou, Lymperis, Lola, and Saridakis [31]. We will refer to their model as the PLLS model. The reason why we study this model is twofold: a) the model serves as a good example worth comparison with another model we study in this paper, and b) the results obtained here are modified due to correcting a numerical mistake of Ref. [31](see footnote 1 on page 6). The PLLS Lagrangian is of the form

$$\mathcal{L} = \left(\frac{g^{\mu\nu}\varphi_{,\mu}\varphi_{,\nu}}{2}\right)^\alpha - U(\varphi), \tag{1}$$

where φ is a scalar field and $\alpha \geq 0$ is a constant. The same form of k-essence has recently been studied in the context of the black-bounce solution [34]. The potential U in Ref. [31] is assumed to be a positive function of φ with a specific inflection point. An inflationary potential with an inflection or near inflection point leads to an ultra slow-roll regime, which in turn leads to a peak in the power spectrum of curvature perturbations on comoving wavenumber scales above the CMB pivot scale q_{CMB}. As a result, the enhanced cosmological perturbations could collapse into PBHs.

Second, we consider the tachyon inflation model [35, 36, 37, 38, 39, 40, 41, 42, 43, 44, 45, 46, 47, 48]. The first proposals for tachyon inflation models date back to the beginning of this century, emerging as promising candidates for a natural mechanism to trigger inflation. In our previous works [46, 49, 50, 51, 52], we have studied tachyon inflation in the contexts of the Randall–Sundrum type braneworld cosmology, and have shown that the predicted observational cosmological parameters are in good agreement with Planck data. In this work, we apply the tachyon inflation model to study the formation of PBHs.

The Tachyon model is motivated by low-energy string theory. The existence of tachyons in the perturbative spectrum of string theory shows that the perturbative vacuum is unstable. This instability implies that there exists a true vacuum to which a tachyon field φ tends [53]. The foundations of this process are given by a model of effective field theory [54] with a Lagrangian of the DBI form

$$\mathcal{L} = -U(\varphi)\sqrt{1 - g^{\mu\nu}\varphi_{,\mu}\varphi_{,\nu}}\,. \tag{2}$$

This model belongs to a wider class of DBI theories described by the Lagrangian [55]

$$\mathcal{L} = -f(\theta)^{-1}\sqrt{1 - f(\theta)g^{\mu\nu}\theta_{,\mu}\theta_{,\nu}} - V(\theta)\,. \tag{3}$$

Making use of a field redefinition $\varphi = \int f(\theta)d\theta$, identifying $f(\theta)^{-1} = U(\varphi)$, and setting $V(\theta) = 0$, yields a transformed Lagrangian of the form (2). A Lagrangian of the form (3) appears in the so-called brane inflation models [27, 56]. In these models, the motion of a D3-brane in a warped throat region of a compact space drives inflation, and the DBI field corresponds to the position of the D3-brane. In Ref. [27], a specific form of the warp factor f is chosen to facilitate the phenomenological oscillating sound speed. In contrast, the tachyon potential U, corresponding to f^{-1} in Eq. (3), is chosen to have an inflection point, as in the PLLS case, and thereby yields enhanced PBH production.

The advantage of the k-essence approach to PBH formation is due to its simple mechanism of ultra-slow-roll dynamics as a consequence of the inflection point. The models of this type yield straightforward predictions easily confronted with observations. Besides, as we show in the last section (see also Refs. [55]), the amplitude of the primordial non-Gaussianity in both PLLS and Tachyon models is well within observational constraints. More generally, the merit of the tachyon model considered here is in its fundamental origin in low-energy string theory and brane dynamics.

To achieve our primary objective, we first calculate the power spectra of the curvature perturbations in the two models mentioned above and demonstrate that the spectra exhibit a substantial enhancement, depending on the input parameters and initial values of the background fields. We calculate the spectra at the acoustic horizon, assuming the Bunch-Davies initial conditions in the deep subhorizon region. Then, using the critical collapse and peaks formalism, we calculate the PBH abundance today that constitutes a fraction of dark matter.

The remainder of the paper is organized as follows. In the next two sections, we investigate the background equations of the PLLS model (Sec. 2) and the Tachyon model (Sec. 3). In Section

4, we study the spectra of curvature perturbations in both models. In Section 5, we present our results on the PBH formation. In the last section, Sec. 6, we summarize our main results and outline conclusions. In Appendix A we outline the procedure for calculating the critical overdensity threshold for collapse.

Notation

We use the metric signature $(+, -, -, -)$. Unless specified otherwise, we use the system of units in which $c = \hbar = 1$. For convenience, we introduce a length scale ℓ so that $\ell \gg 1/M_{\text{Pl}}$, where $M_{\text{Pl}} = \sqrt{1/(8\pi G)}$ is the reduced Planck mass. By $\mathcal{L}$ and $\mathcal{H}$, we denote the Lagrangian and Hamiltonian multiplied by ℓ^4 so that our $\mathcal{L}$ and $\mathcal{H}$ are dimensionless. By φ and ϕ, we denote the scalar fields connected by $\varphi = \ell^2 \phi$ and have the dimension of length and mass, respectively.

2 The PLLS Model

In this section, we briefly recapitulate the model of Ref. [31]. The Lagrangian of this model is a sum of a non-canonical kinetic term and a potential term with inflection,

$$\mathcal{L} = \left(\frac{X}{2}\right)^{\alpha} - U(\varphi), \tag{4}$$

where

$$X = g^{\mu\nu}\varphi_{,\mu}\varphi_{,\nu} \tag{5}$$

is assumed positive. Here, φ is a scalar field of dimension of length, and $\alpha \geq 1$ is a constant. The physical field ϕ, related to φ via

$$\phi = \varphi/\ell^2, \tag{6}$$

has the usual dimension of mass. The potential with inflection proposed in [31] is given by

$$U = \ell^4 V_0 \left[\exp\left(-\lambda \frac{|\varphi_0 - \varphi|^n \text{sgn}(\varphi_0 - \varphi)}{\ell^{2n} M_{\text{Pl}}^n}\right) - \exp\left(-\lambda \frac{\varphi_0^n}{\ell^{2n} M_{\text{Pl}}^n}\right)\right]. \tag{7}$$

The quantity V_0 is a constant of the dimension of mass to the 4th power and λ is a positive dimensionless constant. The field shift φ_0 corresponds to a shift ϕ_0 of the physical field ϕ. This potential has an inflection at $\varphi = \varphi_0$.

The background evolution will be studied using the covariant Hamilton formalism (for details see Ref. [57]). For a general scalar field Lagrangian $\mathcal{L}(\varphi_{,\mu}, \varphi)$, the covariant Hamiltonian $\mathcal{H}(\eta^{\mu}, \varphi)$ is related to $\mathcal{L}$ through the Legendre transformation

$$\mathcal{H}(\eta^{\mu}, \varphi) = \eta^{\mu}\varphi_{,\mu} - \mathcal{L}(\varphi_{,\mu}, \varphi), \tag{8}$$

with conjugate variables satisfying the conditions

$$\varphi_{,\mu} = \frac{\partial \mathcal{H}}{\partial \eta^{\mu}}, \tag{9}$$

$$\eta^{\mu} = \frac{\partial \mathcal{L}}{\partial \varphi_{,\mu}}. \tag{10}$$

By making use of Eqs. (8), (10), and the Euler-Lagrange equation

$$\left(\frac{\partial \mathcal{L}}{\partial \varphi_{,\mu}}\right)_{;\mu} = \frac{\partial \mathcal{L}}{\partial \varphi}, \tag{11}$$

4

we find

$$\eta^{\mu}{}_{;\mu} = -\frac{\partial \mathcal{H}}{\partial \varphi}. \tag{12}$$

Equations (9) and (12) are the covariant Hamilton equations. The most general k-essence Lagrangian is a function of the form $\mathcal{L} = \mathcal{L}(X, \varphi)$, where X is given by (5). From (10) it follows that the quantity

$$\eta^2 = g_{\mu\nu}\eta^{\mu}\eta^{\nu} = 4X(\mathcal{L}_X)^2 \tag{13}$$

is positive. Here, the subscript $_X$ denotes a derivative with respect to X. Then, one can introduce the four-velocity

$$u_{\mu} = \frac{g_{\mu\nu}\eta^{\nu}}{\eta} = \epsilon\frac{\varphi_{,\mu}}{\sqrt{X}}, \tag{14}$$

where, ϵ is $+1$ or -1 according to whether $\varphi_{,0}$ is respectively positive or negative. This choice of ϵ guarantees that u_0 is always positive. The quantity η in (14) is a square root of (13),

$$\eta \equiv 2\epsilon\sqrt{X}\mathcal{L}_X = \epsilon\frac{\partial \mathcal{L}}{\partial \sqrt{X}}. \tag{15}$$

We can regard the variable η as a conjugate to $\sqrt{X}$ as described in [57]. Next, using (8) and (10) one can express $\mathcal{H}$ as a function of X and φ,

$$\mathcal{H} = 2X\mathcal{L}_X - \mathcal{L}. \tag{16}$$

Then, from (13) it follows that X is an implicit function of η^2 and φ which we can (in principle) solve for X to obtain $X = X(\eta^2, \varphi)$. Hence, in a k-essence type of theory, one can regard the Hamiltonian as a function of $\eta^2 = g_{\mu\nu}\eta^{\mu}\eta^{\nu}$ and φ.

Using the definitions of the velocity (14) and expansion rate

$$H \equiv \frac{1}{3}u^{\mu}{}_{;\mu}, \tag{17}$$

the covariant Hamilton equations (9) and (12) can be expressed as

$$\dot{\varphi} = \frac{\partial \mathcal{H}}{\partial \eta}, \tag{18}$$

$$\dot{\eta} + 3H\eta = -\frac{\partial \mathcal{H}}{\partial \varphi}. \tag{19}$$

where a quantity f with an over-dot means $\dot{f} \equiv u^{\mu}f_{,\mu}$. In the comoving frame, the over-dot becomes a derivative with respect to time, and the expansion rate becomes $H = \dot{a}/a$ as usual. For the PLLS Lagrangian (4) we find

$$\mathcal{H} = (2\alpha - 1)\left(\frac{X}{2}\right)^{\alpha} + U(\varphi). \tag{20}$$

In this model, the variable X can be expressed as an explicit function of η. By making use of (4) and (15) we find

$$\frac{X}{2} = \left(\frac{\eta^2}{2\alpha^2}\right)^{1/(2\alpha-1)}. \tag{21}$$

5

Then, we obtain the Hamiltonian expressed in terms of φ and η as

$$\mathcal{H} = (2\alpha - 1)\left(\frac{\eta^2}{2\alpha^2}\right)^{\alpha/(2\alpha-1)} + U(\varphi). \tag{22}$$

As usual, the pressure p and energy density ρ are identified with the Lagrangian and the Hamiltonian, respectively. Then, the Hubble expansion rate H is given by

$$H^2 = \frac{\mathcal{H}}{3\ell^4 M_{\mathrm{Pl}}^2}, \tag{23}$$

and the speed of sound by

$$c_{\mathrm{s}}^2 \equiv \frac{\mathcal{L}_X}{\mathcal{H}_X} = \frac{1}{2\alpha - 1}. \tag{24}$$

The first slow roll parameter is given by

$$\varepsilon_1 \equiv -\dot{H}/H^2 = \frac{\mathcal{L} + \mathcal{H}}{2\ell^4 M_{\mathrm{Pl}}^2 H^2} = \frac{3\alpha\left[\eta^2/(2\alpha^2)\right]^{\alpha/(2\alpha-1)}}{(2\alpha - 1)\left[\eta^2/(2\alpha^2)\right]^{\alpha/(2\alpha-1)} + U(\varphi)}. \tag{25}$$

The higher order slow roll parameters ε_i are defined recursively

$$\varepsilon_{i+1} = \frac{\dot{\varepsilon}_i}{H\varepsilon_i}, \quad i \geq 1. \tag{26}$$

We adopt the convention that inflation ends when either ε_1 or ε_2 is close to unity.

The Hamilton equations (18) and (19) govern the background dynamics. Introducing the e-fold number

$$N = \int dt\, H, \tag{27}$$

it is convenient to rewrite the Hamilton equations (18) and (19) as differential equations with respect to N. In this model we find

$$\frac{d\varphi}{dN} = \frac{\eta}{\alpha H}\left(\frac{\eta^2}{2\alpha^2}\right)^{(1-\alpha)/(2\alpha-1)}, \tag{28}$$

$$\frac{d\eta}{dN} = -3\eta - \frac{1}{H}\frac{\partial U}{\partial \varphi}, \tag{29}$$

where

$$H = \frac{1}{\sqrt{3}\,\ell^2 M_{\mathrm{Pl}}}\left[(2\alpha - 1)\left(\frac{\eta^2}{2\alpha^2}\right)^{\alpha/(2\alpha-1)} + U(\varphi)\right]^{1/2}. \tag{30}$$

The Klein-Gordon equation

Instead of the two first-order Hamilton equations, one can use the second-order field equation of motion. This equation can be obtained directly from the Lagrangian or combining Eqs. (28) and (29). Either way one finds[1]

$$\varphi'' + \left(\frac{3}{2\alpha - 1} - \varepsilon_1\right)\varphi' + \frac{1}{U}\frac{dU}{d\varphi}\frac{3\alpha - (2\alpha - 1)\varepsilon_1}{2\alpha(2\alpha - 1)\varepsilon_1}\varphi'^2 = 0, \tag{31}$$

---

[1]A comparison with Ref. [31] reveals that the factor $\alpha(2\alpha - 1)$ in the denominator of the last term on the left-hand side of Eq. (31) is missing in their equation (2.9).

where

$$\varepsilon_1 = \frac{\alpha}{\ell^2 H^2} \left(\frac{H^2 \varphi'^2}{2} \right)^\alpha,$$ (32)

and H is a solution to

$$\ell^2 H^2 = \frac{1}{\ell^2 M_{\text{Pl}}^2} \left[(2\alpha - 1) \left(\frac{H^2 \varphi'^2}{2} \right)^\alpha + U(\varphi) \right].$$ (33)

Here and from here on, the prime $'$ denotes a derivative with respect to N. The expression (33) is an algebraic equation for the unknown H^2, so the Klein-Gordon equation (31) involves an implicit function $H = H(\varphi, \varphi')$.
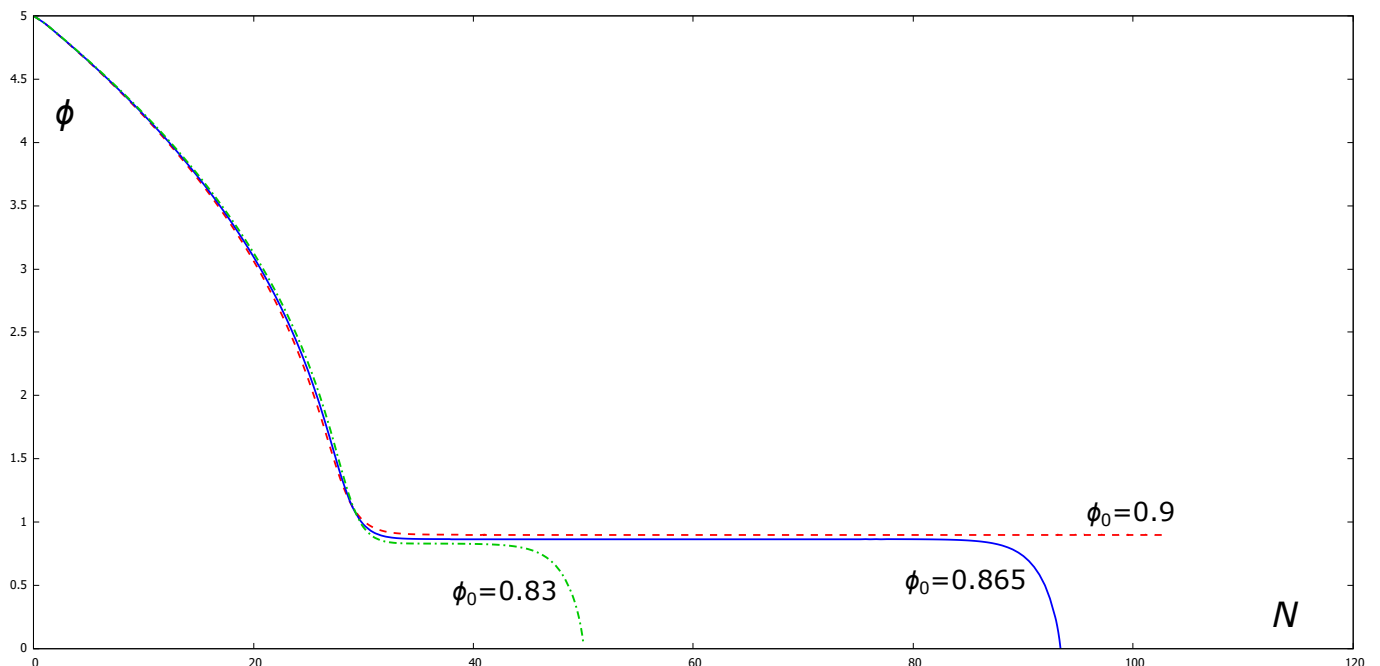
Figure 1: The solution to the Hamilton equations (28) and (29) for the PLLS model. The physical field ϕ in units of M_{Pl} is ploted for $\alpha = 1.5$, fixed initial $\phi_{\text{in}} = 5 M_{\text{Pl}}$, $\phi'_{\text{in}} = -8 \cdot 10^{-7} M_{\text{Pl}}$ and various ϕ_0 in units of M_{Pl}. The remaining parameters $V_0 = 10^{-16} M_{\text{Pl}}^4$ and $\lambda = 7.54 \cdot 10^{-6}$ are as in Ref [31].

Input parameters and initial values

The abundance of PBHs depends crucially on the amplitude of the inflationary power spectrum. The initial curvature perturbations will eventually collapse to form BHs if the peak in the amplitude exceeds a certain threshold, which strongly depends on the shape of the curvature spectrum [9]. To achieve a desirable spectrum, it is necessary to tune the input parameters and initial values. However, the tuning of these parameters is not quite arbitrary since the normalization of the curvature spectrum is constrained by its observational value at the pivot CMB scale. As a starting point, we can use the parameterization of Ref. [31] and fix $\ell = 10^6 M_{\text{Pl}}^{-1}$, $\alpha = 1.5$, $V_0 = 10^{-16} M_{\text{Pl}}^4$, and $\lambda = 7.54 \cdot 10^{-6}$ for $n = 3$.

Regarding the initial values for φ and η, we first choose ϕ_{in} and ϕ'_{in} in units of M_{Pl} as in Ref. [31]. Then, the corresponding initial φ_{in} and φ'_{in} are obtained using $\varphi = \ell^2 \phi$. The corresponding initial η_{in} is obtained by making use of (28) and numerically solving

$$(\varphi'_{\mathrm{in}})^2 = \frac{6}{M_{\mathrm{Pl}}^2} \frac{x^{2/(2\alpha-1)}}{(2\alpha-1)x^{2\alpha/(2\alpha-1)} + U(\varphi_{\mathrm{in}})} \tag{34}$$

for x, where

$$x = -\frac{\eta_{\mathrm{in}}}{\sqrt{2\alpha}}. \tag{35}$$

Following Ref. [31], we tune ϕ_{in} and ϕ'_{in} to obtain a plateau-like behavior as shown in Fig. 1. These plateau-like solutions are required for a significant PBH production, which we will study in Sec. 5.
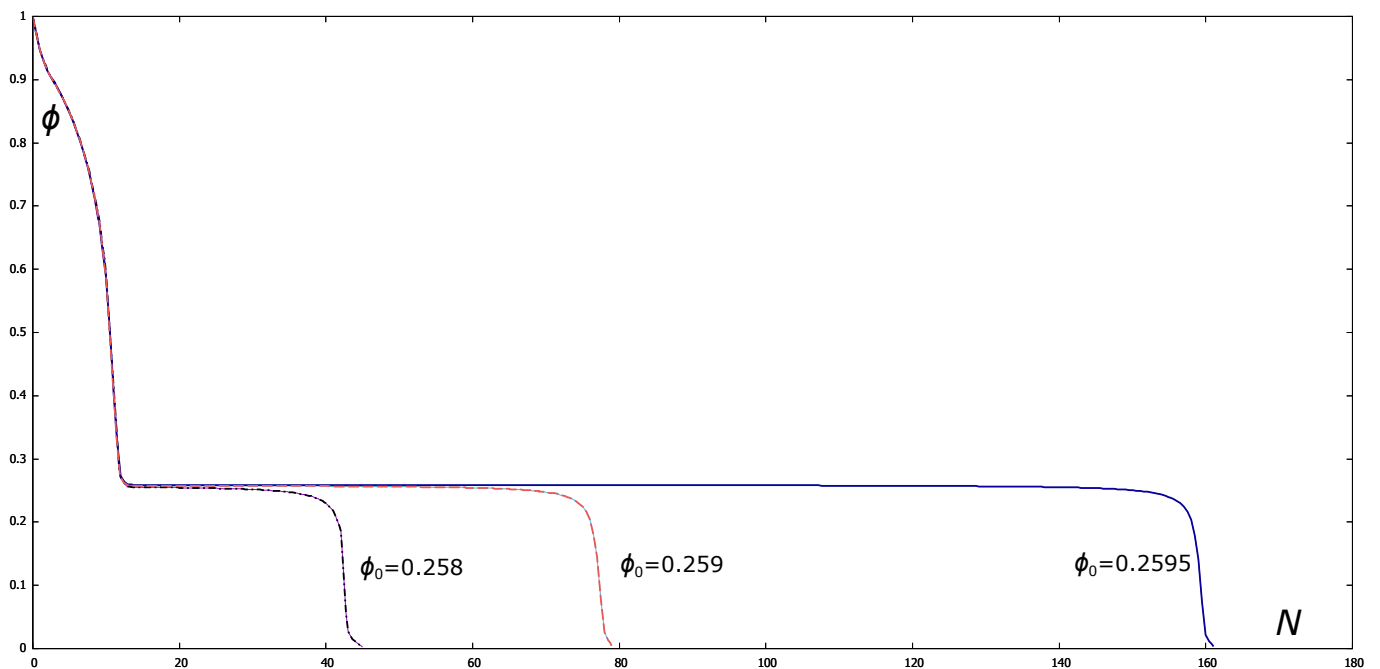

Figure 2: The solution to the Hamilton equations (39) and (40) for the Tachyon model. The physical field ϕ (in units of M_{Pl}) is plotted as a function of N for $\phi_{\mathrm{in}} = 1 M_{\mathrm{Pl}}$, $\eta_{\mathrm{in}} = -3 \cdot 10^3$, $V_0 = 10^{-16} M_{\mathrm{Pl}}^4$, $\lambda = 7.502 \cdot 10^{-6}$, and various field shifts ϕ_0 in units of M_{Pl}, as indicated on the plot.

3 The Tachyon model

The Lagrangian in the Tachyon model is given by

$$\mathcal{L} = -U(\varphi)\sqrt{1-X}, \tag{36}$$

where U is a smooth function of the scalar field φ, and $X \equiv g^{\mu\nu}\varphi_{,\mu}\varphi_{,\nu} > 0$. As before, we introduce the conjugate field η related to X via the definition (15). Using (15) and (36) we obtain X as a function of the fields φ and η
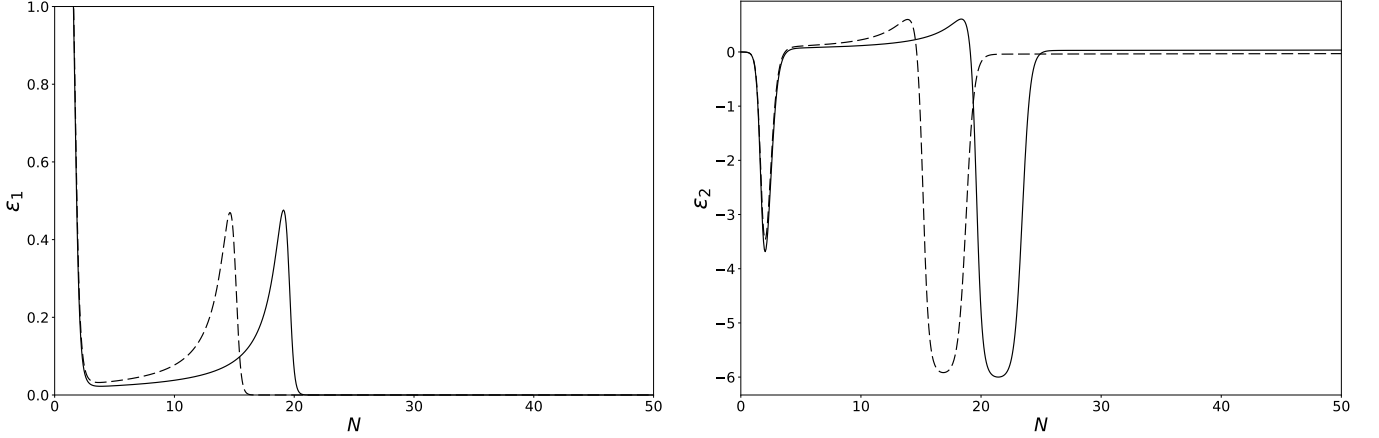
$$X = \frac{\eta^2}{U^2 + \eta^2}. \tag{37}$$

Figure 3: The slow-roll parameters ε_1 (left panel) and ε_2 (right panel) versus N in the Tachyon model for $\phi_{\text{in}} = 1.1 M_{\text{Pl}}$ (full line) and $1.0520 M_{\text{Pl}}$ (dashed line). The remaining corresponding parameters are listed in Table 1.

The Hamiltonian can be expressed as a function of either X or η^2,

$$\mathcal{H} = \frac{U}{\sqrt{1-X}} = \sqrt{U^2 + \eta^2}. \tag{38}$$

Then, the Hamilton equations (18) and (19), expressed as differential equations with respect to N, become

$$\frac{d\varphi}{dN} = \frac{\eta}{H\sqrt{U^2 + \eta^2}}, \tag{39}$$

$$\frac{d\eta}{dN} = -3\eta - \frac{U}{H\sqrt{U^2 + \eta^2}} \frac{\partial U}{\partial \varphi}, \tag{40}$$

where the Hubble expansion rate is given by

$$H^2 = \frac{\sqrt{U^2 + \eta^2}}{3\ell^4 M_{\text{Pl}}^2}. \tag{41}$$

The first slow-roll parameter and the speed of sound squared can be expressed as

$$\varepsilon_1 = \frac{3}{2} X = \frac{3}{2} \frac{\eta^2}{U^2 + \eta^2}, \tag{42}$$

$$c_{\text{s}}^2 = 1 - X = \frac{U^2}{U^2 + \eta^2} = 1 - \frac{2}{3}\varepsilon_1. \tag{43}$$

As in the PLLS model, we choose the potential $U(\varphi)$ defined by (7). The parameters of the potential are $\ell = 10^6 M_{\text{Pl}}^{-1}$, $n = 3$, and $V_0 = 10^{-16} M_{\text{Pl}}^4$ as before. For this model we choose a slightly different $\lambda = 7.502 \cdot 10^{-6}$. Regarding the initial values for φ and η, we first choose ϕ_{in} in units of M_{Pl} of the order of those in Ref. [31] with the corresponding $\varphi_{\text{in}} = \ell^2 \phi_{\text{in}}$. Then, we tune φ_{in} and η_{in} to obtain plateau-like solutions as shown in Fig. 2.

As in the PLLS case, the scalar field exhibits a plateau owing to the inflection point of the potential at $\phi = \phi_0$. As shown in Fig. 2, the extension of the plateau depends on ϕ_0. In this flat

9

region, slow-roll conditions will not be met, and inflation will enter a temporary ultra-slow-roll regime. In Fig. 3 we plot the slow-roll parameters as a function of N. During this period, as we will demonstrate in the next section, the non-constant mode of the curvature fluctuations, which would decay exponentially in the slow-roll regime, actually grows in the ultra-slow-roll regime. As a consequence, the curvature power spectrum will be enhanced at specific scales that can potentially collapse, forming primordial BHs in the early Universe.

4   Curvature perturbations

We start from the 1st-order differential equations of Garriga and Mukhanov [58] expressed in the form [46, 59]

$$a\dot{\xi}_q = z^2 c_{\rm s}^2 \zeta_q, \tag{44}$$

$$a\dot{\zeta}_q = -z^{-2} q^2 \xi_q, \tag{45}$$

where q is the comoving wavenumber and ζ_q is the Fourier transformed curvature perturbation on uniform-density hyper-surfaces. The quantity z^2 can be expressed in different ways:

$$z^2 = \frac{a^2(p+\rho)}{H^2 c_{\rm s}^2} = \frac{2M_{\rm Pl}^2 a^2 \varepsilon_1}{c_{\rm s}^2} = \frac{a^2 \eta \mathcal{H}_{,\eta}}{\ell^4 H^2 c_{\rm s}^2} = \frac{a^2 \mathcal{H}_{,\eta}^2}{\ell^4 H^2 \mathcal{H}_{,\eta\eta}}. \tag{46}$$

Here, the subscripts η and $\eta\eta$ denote respectively the first and second-order partial derivatives with respect to η.

It is convenient to substitute the e-fold number N for t using $dt = dN/H$ and express Eqs. (44)-(45) as differential equations with respect to N. Then, combining the obtained equations, one can derive the Mukhanov-Sasaki second-order differential equation

$$\frac{d^2 \zeta_q}{dN^2} + \left(3 + \varepsilon_2 - \varepsilon_1 - 2\frac{c_{\rm s}'}{c_{\rm s}}\right)\frac{d\zeta_q}{dN} + \frac{c_{\rm s}^2 q^2}{a^2 H^2}\zeta_q = 0. \tag{47}$$

Equation (47) is equivalent to the set (44)-(45) with (46). We will integrate Eq. (47) in conjunction with the background Hamilton equations for the two models considered in Secs. 2 and 3.

The perturbations travel at the speed of sound, and their horizon is the acoustic horizon with radius $c_{\rm s}/H$. At the acoustic horizon, the perturbations with the comoving wave number q satisfy the horizon crossing relation

$$a(N_q)H(N_q) = c_{\rm s}(N_q)q. \tag{48}$$

In the slow-roll regime, the perturbations are conserved once they cross the horizon from the subhorizon to the superhorizon region. A rough estimate [57] shows that the horizon crossing happens at a relatively large q-dependent N of the order $N_q \sim 7 + \ln q/q_{\rm CMB}$, where $q_{\rm CMB}$ is the CMB pivot scale. The curvature perturbations ζ_q are approximately constant at large N once they cross the horizon and enter the superhorizon region where $a(N)H(N) > c_{\rm s}(N)q$, $N > N_q$.

The power spectrum of curvature perturbations is obtained from the two-point correlation function

$$\langle \hat{\zeta}_q \hat{\zeta}_{q'} \rangle = (2\pi)^3 \delta(\boldsymbol{q} + \boldsymbol{q}')|\zeta_q|^2, \tag{49}$$

where $\hat{\zeta}_q$ is the operator associated with the curvature perturbation ζ [60]. We define

$$\mathcal{P}_{\rm S}(q) = \frac{q^3}{2\pi^2}|\zeta_q(N_q)|^2, \tag{50}$$

10

where $\zeta_q(N_q)$ is the solution to Eq. (47) taken at the point N_q which for given q satisfies (48). The curvature perturbation spectrum needs to satisfy the Harrison-Zeldovich spectrum near $q = q_{CMB} = 0.05 \text{ Mpc}^{-1}$

$$\mathcal{P}_S(q) = A_S \left(\frac{q}{q_{CMB}} \right)^{n_S - 1}, \tag{51}$$

where n_S is the scalar spectral index and $A_S = (2.10 \pm 0.03) \times 10^{-9}$. Since the Mukhanov-Sasaki equation (47) is linear, the requirement

$$\mathcal{P}_S(q_{CMB}) = \frac{q_{CMB}^3}{2\pi^2} |\zeta_{q_{CMB}}(N_{q_{CMB}})|^2 = A_S \tag{52}$$

can fix the normalization of ζ_q.

For convenience, instead of ζ_q from now on, we will use the Mukhanov-Sasaki function $v_q = z\zeta_q$, where the quantity z is defined by (46). Then, Eq. (47) may be written as

$$v_q'' + (1 - \varepsilon_1)v_q' + \left[\frac{c_s^2 q^2}{a^2 H^2} - (2 - \varepsilon_1 + \frac{\varepsilon_2}{2} - \frac{c_s'}{c_s})(1 + \frac{\varepsilon_2}{2} - \frac{c_s'}{c_s}) - \frac{\varepsilon_2 \varepsilon_3}{2} + (\frac{c_s'}{c_s})' \right] v_q = 0. \tag{53}$$

Note that in the PLLS model c_s' vanishes whereas in the Tachyon model, we have

$$\frac{c_s'}{c_s} = -\frac{\varepsilon_1 \varepsilon_2}{3 - 2\varepsilon_1}, \tag{54}$$

$$(\frac{c_s'}{c_s})' = -\frac{(\varepsilon_1 \varepsilon_2^2 + \varepsilon_1 \varepsilon_2 \varepsilon_3)(3 - 2\varepsilon_1) + 2\varepsilon_1^2 \varepsilon_2^2}{(3 - 2\varepsilon_1)^2}. \tag{55}$$

Note that Eq. (53) follows from Eqs. (44)-(45) via (46) and (47). Since the derivation of Eqs. (44)-(45) does not involve the slow-roll assumption, the quantities ε_1 and ε_2 that appeear in Eqs. (53)-(55) are not necessarily small. In our numerical integration of Eq. (53) with (54)-(54), we will treat the slow-roll parameters ε_1 and ε_2 as exact background quantities, not subject to the slow-roll conditions.

To solve Eq. (53), we need to choose the initial point $N_{in,q}$ for each wavenumber q. The appropriate q-dependent initial point must be in the deep subhorizon region where $a_{in}H_{in} \ll c_s q$. More precisely, for each wave number q that satisfies the horizon crossing relation $a(N_q)H(N_q) = c_s(N_q)q$, we start at a q-dependent $N_{in,q} < N_q$ such that

$$a(N_{in,q})H(N_{in,q}) = \beta c_s(N_{in,q})q, \tag{56}$$

where β is a small parameter, e.g., $\beta = 0.01$ as proposed in Ref. [61]. Owing to the N-translation invariance of the background equations, we could choose an arbitrary origin of inflation N_0 as an initial point related to a wavenumber $q_0 < q_{CMB}$. In other words, we set

$$a_0 H_0 = \beta c_{s0} q_0 = \epsilon c_{s0} q_{CMB}, \tag{57}$$

where $a_0 = a(N_0)$, $H_0 = H(N_0)$, $c_{s0} = c_s(N_0)$, and the small parameter ϵ satisfies $\epsilon < \beta$, e.g., $\epsilon = 0.001$. Then, using $a = a_0 e^{N - N_0}$ together with (57), we can write the first term in the square brackets in Eq. (53) as

$$\frac{c_s^2 q^2}{a^2 H^2} = \frac{e^{2N_0 - 2N}}{\epsilon^2} \frac{c_s^2}{c_{s0}^2} \frac{H_0^2}{H^2} \frac{q^2}{q_{CMB}^2}. \tag{58}$$

For more details on the choice of the initial point, see Ref. [57].

11

To find the spectrum at the horizon crossing, equation (53) should be integrated for a fixed q up to the e-fold number N_q, which satisfies the horizon-crossing equation (48). Fixing the beginning of inflation at $N_0 = 0$ and combining Eqs. (48) and (57) we obtain

$$e^{N_q} = \frac{1}{\epsilon}\frac{q}{q_{\text{CMB}}}\frac{H_0}{H(N_q)}\frac{c_{\text{s}}(N_q)}{c_{\text{s}0}}, \tag{59}$$

which, given q, may be regarded as an algebraic equation for N_q. The explicit functional dependence $H(N_q)$ and $c_{\text{s}}(N_q)$ in (59) is obtained by integrating the background Hamilton equations in parallel with (53). Then, the spectrum $\mathcal{P}_{\text{S}}(q)$ can be plotted using the solutions $\zeta_q(N_q)$ at the point N_q that satisfies (59) for each q.

Initial conditions

To determine the proper initial conditions in the deep subhorizon region, we adopt the standard Bunch-Davies vacuum solution [62]

$$v_q(\tau) = \frac{e^{-ic_{\text{s}}q\tau}}{\sqrt{2c_{\text{s}}q}}, \tag{60}$$

where the conformal time τ is defined by

$$d\tau = \frac{dt}{a} = \frac{dN}{aH}. \tag{61}$$

Hence, the initial values of v_q and v_q' at $N_{\text{in},q}$ are determined by (60) up to an arbitrary phase. The simplest choice is

$$v_{q\text{in}} \equiv v_q(N_{\text{in},q}) = \frac{1}{\sqrt{2c_{\text{s}}q}}, \tag{62}$$

$$v_{q\text{in}}' \equiv v_q'(N_{\text{in},q}) = -i\frac{c_{\text{s}}q}{a(N_{\text{in},q})H(N_{\text{in},q})\sqrt{2c_{\text{s}}q}}. \tag{63}$$

Then, using (56), we have

$$v_{q\text{in}}' = -i\frac{1}{\beta\sqrt{2c_{\text{s}}q}}, \tag{64}$$

where β is a small constant discussed above, e.g., $\beta = 0.01$. It is understood that the function c_{s} in Eqs. (62)-(64) is taken at $N = N_{\text{in},q}$.

4.1 Redefinition of the input parameters and fields

In our calculations, we assume certain values of the parameters and initial values of the fields. Besides, a solution to Eq. (53) involves the Bunch-Davies initial conditions (62) and (63). These initial conditions determine the normalization of $\zeta_q(N)$ which in turn fixes the normalization of $\mathcal{P}_{\text{S}}$. Hence, there is *a priory* no guarantee that the obtained spectrum will satisfy the condition (52). Instead, the obtained spectrum $\mathcal{P}_{\text{S}}$ will satisfy

$$\mathcal{P}_{\text{S}}(q_{\text{CMB}}) = \frac{A_s}{c_0}, \tag{65}$$

where c_0 is a constant, generally $c_0 \neq 1$. Thus, we have a conflict between the imposed Bunch-Davies vacuum and the normalization of the spectrum to the observed value at the CMB pivot scale.

Table 1: Input parameters and fields

PLLS model, $\alpha = 1.5$		Tachyon model	
original	redefined	original	redefined
U	$c_0^{-1}U$	U	$c_0^{-1}U$
λ	$c_0^{(1-\alpha)/(2\alpha)}\lambda$	λ	$c_0^{-1/2}\lambda$
φ	$c_0^{(\alpha-1)/(2\alpha)}\varphi$	φ	$c_0^{1/2}\varphi$
η	$c_0^{(1-2\alpha)/(2\alpha)}\eta$	η	$c_0^{-1}\eta$

To rectify this conflict, we need to properly redefine the input parameters and initial values. Using an arbitrary constant c_0, one may easily show [57] that the Hamilton equations and the corresponding solutions are invariant under the simultaneous rescaling of the parameters and initial values as shown in Table 1. In both models, the Hubble rate scales according to $H \to c_0^{-1/2}H$ and the rescaled Hamilton equations retain their original form with no dependence on c_0.

We will use this scaling property of our k-essence models to eliminate the constant c_0 in Eq. (65) by redefining the input parameters. To begin, we multiply the right-hand side of (50) by c_0 and write the power spectrum $\mathcal{P}_\mathrm{S}$ as

$$\mathcal{P}_\mathrm{S} = c_0 \frac{q^3}{2\pi^2}|\zeta_q(N_q)|^2 = \frac{c_0 H^2}{4\pi^2 \varepsilon_1 M_\mathrm{Pl}^2}q|v_q|^2, \tag{66}$$

where we have used Eqs. (46) and (48). Now we absorb c_0 in H^2 and rescale the Hubble rate as $H \to c_0^{-1/2}H$. This rescaling does not affect Eq. (53) and its solution v_q. Thus, we obtain a properly normalized spectrum without the c_0 factor. However, a rescaling of H implies a redefinition of the model input parameters and initial values of the background fields. Using the rescaling defined in Table 1 we infer a redefinition of the parameters.

In this way, if we repeat the calculations using the redefined input parameters listed in Table 1 for both models, we will obtain the power spectra that agree with the observed value at the CMB pivot scale.

4.2 Approximate spectrum

In the slow-roll regime, the curvature spectrum can be approximated by (see, e.g., Ref. [59])

$$\mathcal{P}_\mathrm{S}(q) \simeq \frac{1}{8\pi^2 c_\mathrm{s}\varepsilon_1}\frac{H^2}{M_\mathrm{Pl}^2}, \tag{67}$$

where for each q, the quantities H, c_s, and ε_1 take on their horizon crossing values at the corresponding N_q. It is important to stress that in the models considered here the perturbations evolve through a phase which departs from the slow-roll regime, as is evident from Fig. 3. Nevertheless, we will use (67) for the sake of comparison. However, we expect a substantial departure of the power spectrum (67) from the exact one obtained by numerically integrating Eq. (53).

The approximate spectrum obtained in this way will not in general have the correct observed value at the pivot scale q_CMB. To satisfy the proper normalization of $\mathcal{P}_\mathrm{S}(q)$ at $q = q_\mathrm{CMB}$, we can introduce a constant factor $\bar{c}_0$. To wit, we define

$$\mathcal{P}_\mathrm{S}(q) \simeq \frac{\bar{c}_0}{8\pi^2 c_\mathrm{s}\varepsilon_1}\frac{H^2}{M_\mathrm{Pl}^2} \tag{68}$$
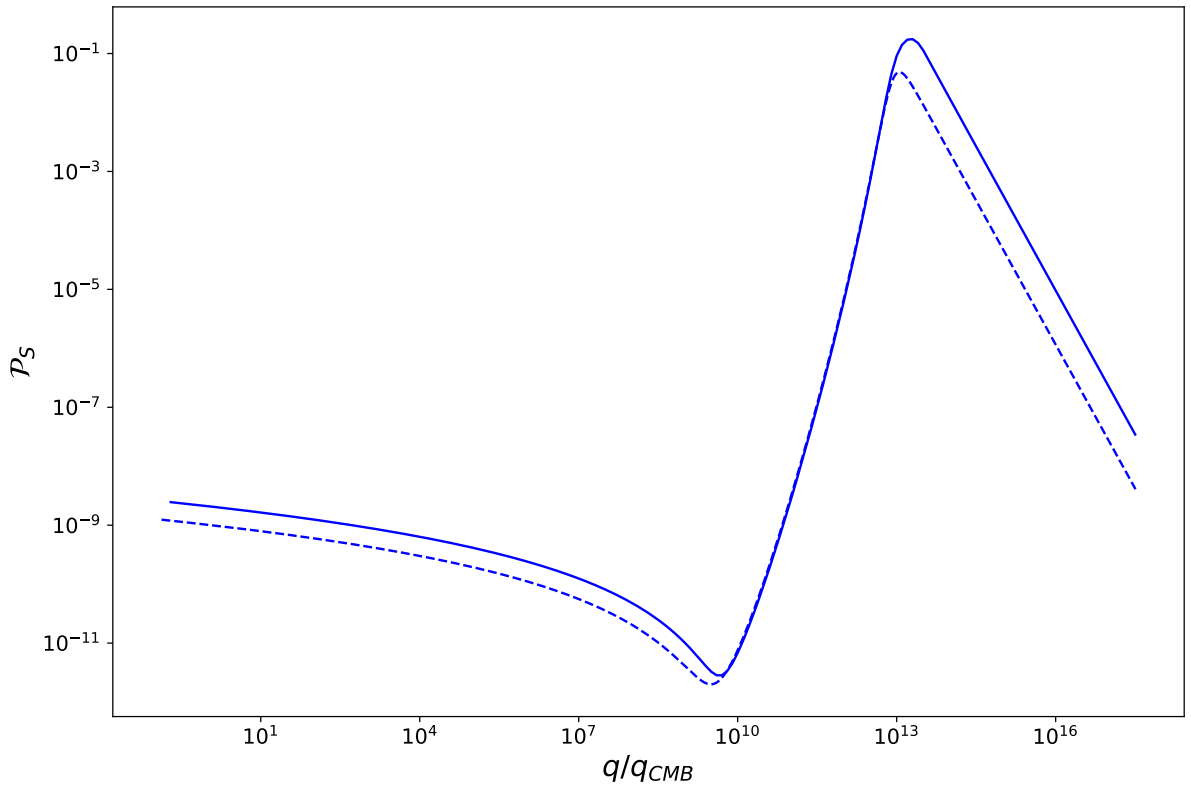
Figure 4: The curvature power spectrum obtained by numerically solving Eq. (53) (full line) and the spectrum approximated by Eq. (68) (dashed line) for the PLLS inflation model with $n = 3$, $\phi_0 = 0.8354 M_{\mathrm{Pl}}$, and $\alpha = 1.5$. The values of V_0 and λ are as in Fig. 1. The initial values are $\phi_{\mathrm{in}} = 5.20473 M_{\mathrm{Pl}}$, $\eta_{\mathrm{in}} = -2.81744 \cdot 10^{-7}$. The initial perturbation $v_{q\mathrm{in}}$ is determined by the Bunch-Davies vacuum and $\mathcal{P}_{\mathrm{S}}(q_{\mathrm{CMB}})$ as discussed in the text.
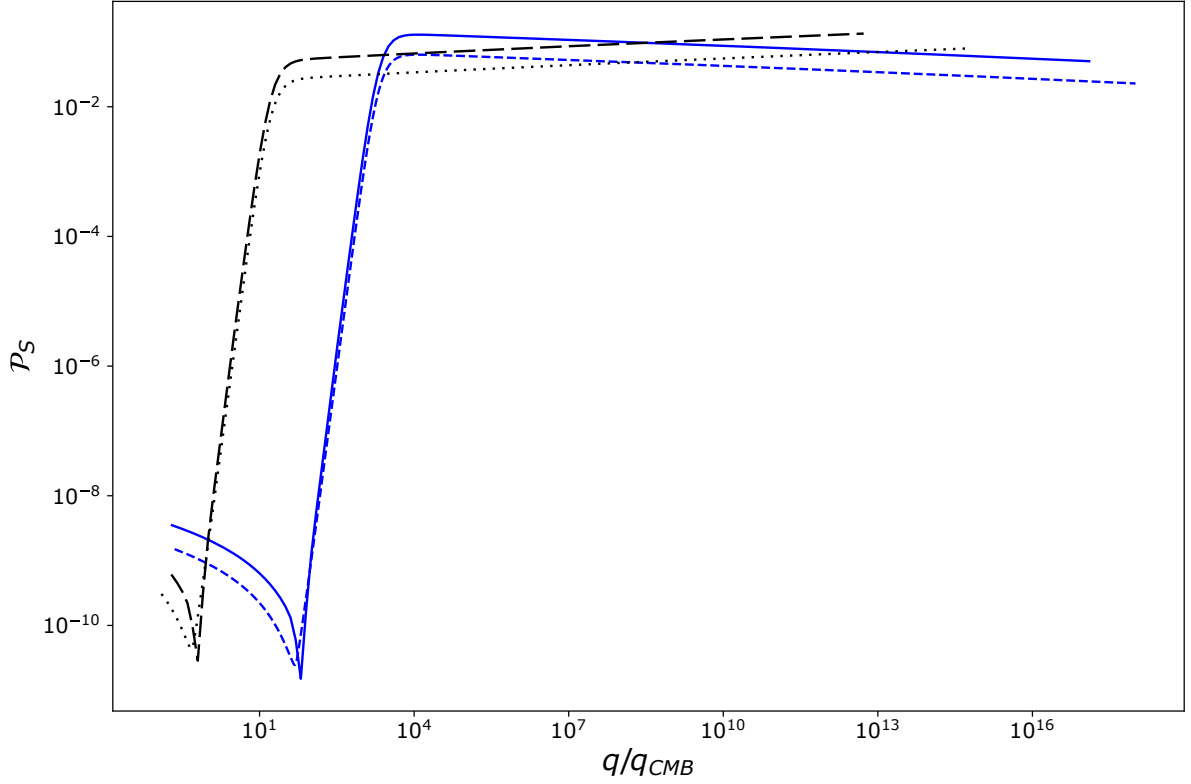
Figure 5: The curvature power spectrum obtained by numerically solving equation (53) (full blue and long-dashed black lines) combined with the spectrum approximated by Eq. (68) (short dashed blue and dotted black lines) for the Tachyon model inflation with the potential U as in the PLLS model. The parameters and initial values of the corresponding background solutions are $\phi_0 = 0.2595 M_{\text{Pl}}$, $V_0 = 10^{-16} M_{\text{Pl}}^4$, $\lambda = 7.502 \cdot 10^{-6}$, $\phi_{\text{in}} = 1.1 M_{\text{Pl}}$, and $\eta_{\text{in}} = -5.3 \cdot 10^4$ (full and short-dashed lines), and $\phi_0 = 0.259831 M_{\text{Pl}}$, $V_0 = 10^{-16} M_{\text{Pl}}^4$, $\lambda = 7.600 \cdot 10^{-6}$, $\phi_{\text{in}} = 1.052 M_{\text{Pl}}$ and $\eta_{\text{in}} = -5.3625 \cdot 10^4$ (long-dashed and dotted lines).

and fix $\bar{c}_0$ so that $\mathcal{P}_S(q_{\text{CMB}})$ has the correct observed value at the pivot scale. However, a choice $\bar{c}_0 \neq 1$ is not compatible with the assumed Bunch-Davies asymptotic behavior. As before, this problem is resolved by absorbing $\bar{c}_0$ in H^2 and redefining the physical parameters as shown in Table 1.

Nota Bene: The constants c_0 and $\bar{c}_0$ need not be necessarily equal. However, to compare the exact and approximate spectra, we must stick to the same parameterization of the model in both exact and approximate calculations. In this case, we will replace $\bar{c}_0$ in (68) by c_0 so that the redefinition of parameters and initial values will be the same. Obviously, in this case, the approximate spectrum will fail to reproduce the correct observed value at $q = q_{\text{CMB}}$.

We plot the calculated spectrum for the PLLS model in Fig. 4. In Fig. 5, we plot the spectra calculated for the Tachyon model for two sets of parameters. The approximation (67) correctly reproduces the shape of the spectrum but underestimates the peak by a factor of the order of 10 and violates the normalization condition (52) (see the note after Eq. (68)).

5 PBH formation

In the radiation-dominated epoch, PBHs could form by small-scale cosmological perturbations with sufficiently large overdensities collapsing after re-entering the cosmological horizon. Assuming spherical symmetry, such regions can be described by the following approximate form of the metric at superhorizon scales [8]

$$ds^2 = dt^2 - a(t)^2 e^{2\zeta(r)}(dr^2 + r^2 d\Omega^2). \tag{69}$$

The quantity $\zeta(r)$ is spherically symmetric comoving curvature perturbation conserved on superhorizon scales [63]. The corresponding density contrast $\delta_r \equiv \delta\rho/\rho(r,t)$ is given by [9]

$$\delta_r = -\frac{8}{9}\frac{1}{a^2 H^2}e^{-5\zeta(r)/2}\nabla^2 e^{\zeta(r)/2}, \tag{70}$$

Keeping the linear terms only, we find

$$\delta_r \simeq -\frac{4}{9}\frac{1}{a^2 H^2}\nabla^2 \zeta(r). \tag{71}$$

In the momentum space we obtain

$$\delta_q \simeq \frac{4}{9}\frac{q^2}{a^2 H^2}\zeta_q. \tag{72}$$

Hence, the two-point correlation function (49) dominates the power spectrum of the density contrast via the linear relation (72). We find

$$P_\delta \equiv \frac{q^3}{2\pi^2}|\delta_q|^2 = \frac{q^3}{2\pi^2}\left(\frac{4}{9}\right)^2\frac{q^4}{a^4 H^4}|\zeta_q|^2 = \left(\frac{4}{9}\right)^2\frac{q^4}{a^4 H^4}\mathcal{P}_S. \tag{73}$$

In our analysis, we assume that both the density contrast δ and curvature perturbation ζ are approximately Gaussian variables. In principle, a non-Gaussian contribution to the statistics of the primordial curvature perturbations could modify the PBH abundance. We will provide a brief comment on non-Gaussianity at the end of this section.

As we will shortly see, the PBH mass fraction $\beta(M)$ will be mainly described by the smoothed variance σ of the density contrast δ, with rough functional dependence as

$$\beta \propto \left(-\frac{\delta_c}{2\sigma^2}\right), \tag{74}$$

16

where δ_c is the critical overdensity collapse threshold. Hence, the larger the variance σ, the larger the mass fraction β. We define the smoothed variance of δ over the smoothing scale $R = 1/(aH)$

$$\sigma(R)^2 = \int_0^\infty \frac{dq}{q} W(q,R)^2 \mathcal{P}_\delta = \left(\frac{4}{9}\right)^2 \int_0^\infty \frac{dq}{q} (Rq)^4 W(q,R)^2 \mathcal{P}_S \tag{75}$$

and the first moment of the smoothed power spectrum

$$\mu(R)^2 = \int_0^\infty \frac{dq}{q} (Rq)^2 W(q,R)^2 \mathcal{P}_\delta = \left(\frac{4}{9}\right)^2 \int_0^\infty \frac{dq}{q} (Rq)^6 W(q,R)^2 \mathcal{P}_S, \tag{76}$$

where W is a smoothing window function. It is not obvious what the best choice for the smoothing function is. There is a priori no reason to choose one smoothing over another [64, 65]. A common convenient choice is a Gaussian window function, although a top-hat smoothing function was occasionally used in the past [66, 67]. However, the top-hat window function is sensitive to scales well within the horizon [68] which requires careful treatment [69, 70].

Ando, Inomata, and Kawasaki [71] investigated the dependence of the variance $\sigma(R)$ on the choice between x-space top hat, gaussian, and k-space top hat window function (see also Refs. [72, 73]). In particular, for a simple scale invariant power spectrum $\mathcal{P}_S = A_S$, they found that the variances $\sigma(R)$ differ in proportions 1:0.29:0.22 for the x-space top hat, Gaussian, and k-space top hat window functions, respectively. We have also checked the window function dependence of $\sigma(R)$ assuming a gaussian shape power spectrum $\mathcal{P}_S(q) \propto \exp[-R^2(q-R_0^{-1})^2/2]$ peaked at various R_0^{-1}. For example, for $R_0 = R$, we have found the proportions 1:0.36:0.27 for the mentioned window functions, respectively. These proportions do not change significantly with varying R_0 in the interval 0.3 - 10, where they remain roughly 1:1/3:1/4.

Following Green et al. [68], we choose gaussian

$$W(q,R) = e^{-q^2 R^2/2}, \tag{77}$$

as a more conservative choice than the x-space top-hat window function.

Toy model

For an illustration, it is useful to consider a flat power spectrum parameterized as

$$\mathcal{P}_S \simeq \mathcal{P}_0 \Theta(q - q_{min}) \Theta(q_{max} - q). \tag{78}$$

This power spectrum, which was studied previously in the literature as a toy model (see, e.g., [74]), can serve as a rough approximation to the Tachyon model power spectrum of Fig. 5 with $\mathcal{P}_0 \simeq 0.1$ - 0.2, $q_{min} = 10^4 q_{CMB}$, and $q_{max} = 10^{16} q_{CMB}$.

Using this in (75) and (76) we obtain

$$\sigma^2 = \frac{1}{2}\left(\frac{4}{9}\right)^2 \mathcal{P}_0 \left[\left(1 + q_{min}^2 R^2\right) e^{-q_{min}^2 R^2} - \left(1 + q_{max}^2 R^2\right) e^{-q_{max}^2 R^2}\right], \tag{79}$$

$$\mu^2 = \frac{1}{2}\left(\frac{4}{9}\right)^2 \mathcal{P}_0 \left[\left(2 + 2q_{min}^2 R^2 + q_{min}^4 R^4\right) e^{-q_{min}^2 R^2} - \left(2 + 2q_{max}^2 R^2 + q_{max}^4 R^4\right) e^{-q_{max}^2 R^2}\right]. \tag{80}$$

The functions $\sigma(R)$ and $\mu(R)$ have a top-hat shape with plateau heights $\sigma_{max} \simeq (4/9)\sqrt{\mathcal{P}_0/2}$ and $\mu_{max} \simeq (4/9)\sqrt{\mathcal{P}_0}$. For R satisfying $1/q_{max} \ll R \ll 1/q_{min}$ we have

$$\sigma = \frac{4}{9}\sqrt{\frac{\mathcal{P}_0}{2}} \left(1 + q_{min}^2 R^2 + \mathcal{O}(q_{min}^4 R^4)\right), \tag{81}$$

17

and hence, the maximal value of sigma is

$$\sigma_{\max} \simeq \frac{4}{9}\sqrt{\frac{\mathcal{P}_0}{2}}. \tag{82}$$

In this range of R, we also have

$$\frac{\mu}{\sigma} \simeq \sqrt{2} + \mathcal{O}(q_{\min}^4 R^4). \tag{83}$$

Functional dependence $R(M)$

Through (75), the variance σ is a function of the comoving horizon radius at the PBH formation time $R = (a_f H_f)^{-1} = 1/q_f$, where the subscript f refers to the PBH formation time. Since the PBH mass M at the formation time is of the order of the cosmological horizon mass, i.e.,

$$M \simeq M_{H_f} = \frac{4\pi}{3}H_f^{-3}\rho_f = \frac{4\pi M_{\text{Pl}}^2}{H_f}, \tag{84}$$

we can relate R to M. From now on, we identify $M \equiv M_{H_f}$.

As a first step, we derive the PBH mass M as a function of the comoving wave number q_f at the PBH formation time. Combining the entropy conservation $S = C_1 g_* T^3 a^3 = \text{const}$ with radiation energy density $\rho_{\text{rad}} = C_2 g_* T^4$, we find

$$\frac{\rho_{\text{rad,f}}}{\rho_{\text{rad,0}}} = \left(\frac{g_{*,0}}{g_{*,f}}\right)^{1/3}\left(\frac{a_0}{a_f}\right)^4, \tag{85}$$

where the quantity g_* is the time-dependent number of effective massless degrees of freedom. Then, from the first Friedmann equation it follows that the Hubble rate H_f at the formation time is related to the Hubble rate H_0 at present as

$$H_f = H_0 \Omega_{\text{rad,0}}^{1/2}(a_0/a_f)^2(g_{*,0}/g_{*,f})^{1/6}, \tag{86}$$

where $\Omega_{\text{rad,0}} = \rho_{\text{rad,0}}/\rho_{\text{crit}}$, with $\rho_{\text{crit}} = 3M_{\text{Pl}}^2 H_0^2$. Combining this with the horizon-crossing relations $q_f = a_f H_f$ and $q_0 = a_0 H_0$, we find

$$\frac{a_f}{a_0} = \Omega_{\text{rad,0}}^{1/2}\left(\frac{g_{*,0}}{g_{*,f}}\right)^{1/6}\frac{q_0}{q_f}. \tag{87}$$

Next, substituting H_f from (86) and a_f from (87) in $M = 4\pi M_{\text{Pl}}^2/H_f$, we find

$$M = \frac{4\pi M_{\text{Pl}}^2}{H_0}\Omega_{\text{rad,0}}^{1/2}\left(\frac{g_{*,0}}{g_{*,f}}\right)^{1/6}\left(\frac{q_0}{q_f}\right)^2 = 1.90\cdot 10^{15}\left(\frac{q_{\text{CMB}}}{q_f}\right)^2 M_\odot. \tag{88}$$

For the numerical estimate in (88), we have used $M_{\text{Pl}} = 2.17645/\sqrt{8\pi}\times 10^{-8}$ kg, $\Omega_{\text{rad,0}} = 10^{-5}$, the Hubble radius today $1/H_0 = 1.2\cdot 10^{26}$ m, $g_{*,f} = 106.75$, $g_{*,0} = 3.36$ (see, e.g., Kolb and Turner [75]), and the solar mass $M_\odot = 2\cdot 10^{30}$ kg.

Finally, using (88) with $a_0 = 1$ we find

$$R \equiv \frac{1}{q_f} = \frac{M^{1/2}}{(4\pi H_0)^{1/2}M_{\text{Pl}}}\left(\frac{g_{*,f}}{g_{*,0}}\right)^{1/12}\Omega_{\text{rad,0}}^{-1/4}. \tag{89}$$

It is convenient to express R as a function of $M/M_\odot$,

$$R = 1.4163\cdot 10^{16}\left(\frac{M}{M_\odot}\right)^{1/2}\text{ m} = 4.590\cdot 10^{-7}\left(\frac{M}{M_\odot}\right)^{1/2}\text{ Mpc}. \tag{90}$$

.

Estimate of the mass range

Suppose the spectrum is significant between q_{min} and q_{max} as in the toy model (78). Inspired by the Tachyon model inflation spectrum depicted in Fig. 5 we use $q_{min} = 10^4 q_{CMB}$, $q_{max} = 10^{16} q_{CMB}$. Then, the BH production will be suppressed for $R > R_{max} = 1/q_{min}$ and $R < R_{min} = 1/q_{max}$. The masses corresponding to R_{min} and R_{max} are

$$M_{min} = \left(\frac{R_{min}}{4.59 \cdot 10^{-7}}\right)^2 \simeq 1.91 \cdot 10^{-17} M_\odot, \tag{91}$$

$$M_{max} = \left(\frac{R_{max}}{4.59 \cdot 10^{-7}}\right)^2 \simeq 1.91 \cdot 10^7 M_\odot. \tag{92}$$

Then, according to (79), the function $\sigma(M)$ will have an approximate top hat profile with M ranging from M_{min} to M_{max} and the top value σ_{max} defined by (82).

5.1 PBH mass fraction

The density of PBHs of mass M at the formation time is a fraction $\beta(M)$ of the total background density $\rho_{rad,f}$,

$$\rho_{PBH,f} = \beta(M)\rho_{rad,f}. \tag{93}$$

We now describe two ways of calculating $\beta(M)$ that appear in the literature: The Press-Schechter and the Critical collapse and peaks (CCP) formalism, and compare the two approaches using the toy-model spectrum.

5.1.1 Press-Schechter (PS) formalism

In the Press-Schechter formalism of gravitational collapse, the mass fraction of PBHs of mass M is described by the probability that the overdensity δ is above a certain threshold value δ_c for collapse. Assuming δ is a Gaussian random variable with mass (or scale) dependent variance, the mass fraction $\beta(M)$ at the time of formation is then given by [76, 77, 78]

$$\beta(M) = \frac{1}{2}\mathrm{erfc}\left(\frac{\delta_c}{\sqrt{2}\sigma}\right) \equiv \frac{1}{\sqrt{2\pi}\sigma}\int_{\delta_c}^{\infty} d\delta \exp\left(-\frac{\delta^2}{2\sigma^2}\right). \tag{94}$$

This function can be approximately expressed in terms of elementary functions by [79]

$$\beta(M) \simeq \frac{\exp\left(-\delta_c^2/(2\sigma^2)\right)}{\sqrt{\pi}\delta_c/(\sqrt{2}\sigma) + \sqrt{\pi\delta_c^2/(2\sigma^2) + 4}}. \tag{95}$$

5.1.2 Critical collapse and peaks (CCP) formalism

Given linear density contrast δ, the PBH mass can be well approximated by the scaling law for critical collapse [80, 81]

$$M_{PBH}(\delta) = KM(\delta_m(\delta) - \delta_c)^\gamma, \tag{96}$$

where δ_m is the smoothed density contrast, $M \equiv M_{H_f}$ is the mass within the cosmological horizon at the PBH formation time t_f in radiation era, and $\gamma \simeq 0.36$ is the critical exponent at t_f [82].

The parameter $K \simeq 4$ depends on the specific profile of the collapsing overdensity. The smoothed density contrast δ_m may be expressed in terms of δ as [81]

$$\delta_m = \delta - \frac{3}{8}\delta^2. \tag{97}$$

Then, the PBH mass fraction is [81]

$$\beta(M) = \int_{\delta_-}^{4/3} d\delta \frac{M_{\text{PBH}}(\delta)}{M} N(\delta), \tag{98}$$

where

$$N(\delta) = \frac{1}{4\pi^2} \left(\frac{\mu\delta}{\sigma^2}\right)^3 \exp\left(-\frac{\delta^2}{2\sigma^2}\right) \tag{99}$$

and the lower integral bound

$$\delta_- = \frac{4}{3}\left(1 - \sqrt{1 - \frac{3}{2}\delta_c}\right) \tag{100}$$

is the smaller root of the quadratic equation

$$\delta - \frac{3}{8}\delta^2 - \delta_c = 0. \tag{101}$$

Then, using (96) with $K = 4$ and (97), we obtain

$$\beta(M) = \frac{1}{\pi^2}\frac{\mu^3}{\sigma^7} \int_{\delta_-}^{4/3} d\delta \left(\delta - \frac{3}{8}\delta^2 - \delta_c\right)^\gamma \delta^3 \exp\left(-\frac{\delta^2}{2\sigma^2}\right). \tag{102}$$

5.1.3 Comparison

The CCP formalism is generally considered to be more refined [65, 83] compared with the PS. Whereas the PS formalism has one universal condition that the density must be above the threshold value, the CCP formalism introduces an additional constraint: PBHs form at peaks of the density [64, 81]. In particular, as pointed out in Ref. [84], the wide variety of the threshold value implies the difficulty in the PS approach: the PBH formation criterion is not a simple matter of the universal threshold for a one-point value of some averaged random field, but we need to deal with the spatial dependence of the local overdensity profile. The two methods have been compared in a comprehensive recent analysis by Yoo et al. [85] (see also Pi et al. [86]) that takes into account the mutually related issues of PBH formation criterion, statistical treatment of non-linear variables, and use of a window function.

To compare these two methods quantitatively, we can use the toy-model spectrum (78). In this model, the function $\beta(M)$ may be approximated by a similar top-hat profile

$$\beta(M) = \beta_0 \Theta(M - M_{\text{min}})\Theta(M_{\text{max}} - M), \tag{103}$$

where the height β_0 can be estimated using either (95) or (102). By way of example, we will use $\gamma = 0.36$, $\delta_c = 0.56$, and $\sigma = (4/9)\sqrt{\mathcal{P}_0/2}$ with $\mathcal{P}_0 = 0.2$ or 0.4. Then, using (102) we obtain $\beta_0 = 1.536 \cdot 10^{-7}$ for $\mathcal{P}_0 = 0.2$ and $3.429 \cdot 10^{-5}$ for $\mathcal{P}_0 = 0.4$. In contrast, using (95) we obtain $\beta_0 = 3.441 \cdot 10^{-5}$ and $2.489 \cdot 10^{-3}$ for $\mathcal{P}_0 = 0.2$ and $\mathcal{P}_0 = 0.4$, respectively. Hence, for a broad power spectrum similar to the toy-model spectrum (78), one may expect that the PS prediction

based on Eq. (95) will be by about a factor of 100 larger than the prediction of the CCP formalism based on Eq. (102).

For the reasons stated above, in the following, we will use the more conservative CCP formalism. However, it is fair to mention that the quantitative difference between the two methods could be reduced by an effective calibration — for example, by adjusting the collapse threshold δ_c or redefining σ so that PS and CCP results become more consistent. In our example above, the height of the mass fraction β_0 decreases very quickly with decreasing $\mathcal{P}_0$, to wit, with decreasing σ. Hence, using different window functions in the two approaches and thereby redefining σ could reduce disagreement between PS and CCP methods. In a recent study [86], it has been shown that incorporating a smoothing procedure into the peak theory framework alleviates the tension between peaks theory and the Press–Schechter formalism.

5.2 PBH abundance

The abundance of PBHs with mass in the interval $(M, M + dM)$ related to the total dark matter (DM) today is defined as [76, 81, 87, 24, 88, 89]

$$\frac{d\Omega_{\text{PBH},0}}{\Omega_{\text{DM},0}} = f_{\text{PBH}} d\ln M. \tag{104}$$

Here, f_{PBH} is the mass-dependent PBH fraction defined as

$$f_{\text{PBH}} \equiv \frac{\rho_{\text{PBH},0}}{\Omega_{\text{DM},0}\rho_{\text{crit}}} = \frac{\rho_{\text{PBH},f}}{\Omega_{\text{DM},0}\rho_{\text{crit}}}\left(\frac{a_f}{a_0}\right)^3 = \frac{\beta(M)\rho_{\text{rad},f}}{\Omega_{\text{DM},0}\rho_{\text{crit}}}\left(\frac{a_f}{a_0}\right)^3, \tag{105}$$

where $\Omega_{\text{DM},0}$ is the fraction of DM today. We have taken into account that PBHs behave like matter, i.e., $\rho_{\text{PBH},0}a_0^3 = \rho_{\text{PBH},f}a_f^3$ and that the PBH density at the formation time is a fraction $\beta(M)$ of the total background density $\rho_{\text{rad},f}$. Substituting $\rho_{\text{rad},f}$ from entropy conservation (85), a_f/a_0 from (87), and q_f/q_0 from (88), we obtain

$$f_{\text{PBH}} = \frac{\beta(M)\Omega_{\text{rad},0}^{3/4}}{\Omega_{\text{DM},0}}\left(\frac{g_{*,0}}{g_{*,f}}\right)^{1/4}\left(\frac{M_0}{M}\right)^{1/2}, \tag{106}$$

where

$$M_0 = 4\pi M_{\text{Pl}}^2/H_0 \tag{107}$$

is the mass of the present cosmological horizon. If we use $g_{*,0} = 3.36$, $\Omega_{\text{rad},0} = 10^{-5}$, $\Omega_{\text{DM},0} = 0.265$, $H_0 = 70\,\text{km}\,\text{s}^{-1}\text{Mpc}^{-1}$, and $M_\odot = 2 \cdot 10^{30}$ kg, we find

$$f_{\text{PBH}} = \frac{\beta(M)}{1.67 \cdot 10^{-8}}\left(\frac{M_\odot}{M}\right)^{1/2}\left(\frac{106.75}{g_{*,f}}\right)^{1/4}. \tag{108}$$

PBH abundance in the top-hat model

For an estimate based on the top-hat toy model, we use $\beta(M)$ defined by (103) with mass range $(M_{\text{min}}, M_{\text{max}})$ defined by (91) and (92) and β_0 calculated in Sec. 5.1 for a chosen $\mathcal{P}_0$. Obviously, the values $\mathcal{P}_0$ and q_{max} (or the corresponding M_{min}) are decisive since $\beta(M)$ is extremely sensitive to $\mathcal{P}_0$ and since f_{PBH} peaks just above M_{min}.
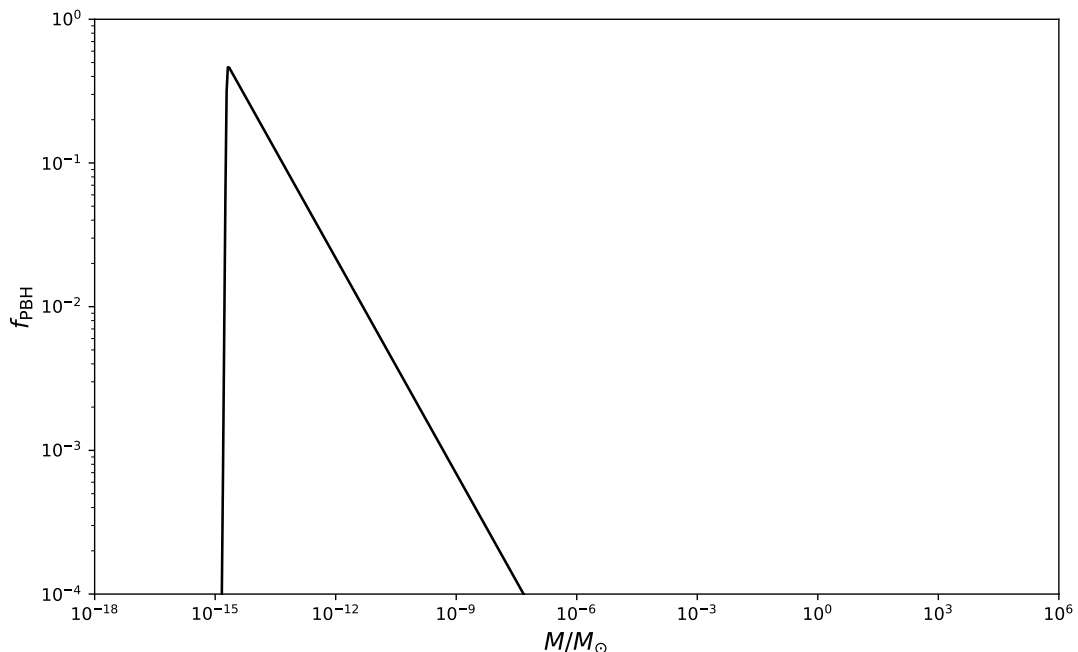
Figure 6: The fraction of PBH dark matter versus M for the flat power spectrum (78) with $q_{min} = 10^4 q_{CMB}$, $q_{max} = 10^{15} q_{CMB}$, and $\mathcal{P}_0 = 0.08866$.

As an example, we take $q_{max} = 10^{15} q_{CMB}$ corresponding to $M_{min} = 1.91 \cdot 10^{-15} M_{\odot}$ and we use the approximate expression (103) with β_0 estimated using (102). Then, for $\mathcal{P}_0 = 0.2$ we find $\beta_0 = 1.536 \cdot 10^{-7}$ and $f_{PBH,peak} = 2.105 \cdot 10^8$, whereas for $\mathcal{P}_0 = 0.08866$ we obtain $\beta_0 = 3.6537 \cdot 10^{-16}$ and $f_{PBH,peak} = 0.50061$. In Fig. 6, we plot the fraction of PBH dark matter as a function of M at the formation time for the top-hat power spectrum (78) with height $\mathcal{P}_0 = 0.08866$. The choice of q_{max} in the top-hat profile is crucial since the position M_{min} of the DM fraction peak is proportional to $1/q_{max}^2$ (Eq. (91)). There exists a natural cutoff at about $q_{max} \sim 10^{17} q_{CMB}$ which corresponds to $M_{min} \simeq 10^{-18} M_{\odot} \simeq 10^{15}$ g. The PBHs of masses smaller than this would have evaporated completely until today.

PBH abundance in the PLLS and Tachyon models

In Fig. 7, we plot the fraction of PBH dark matter as a function of M for the power spectra approximated by equation (68) for both the PLLS and the Tachyon models. The theoretical curves correspond to the power spectra calculated using specifically tuned input parameters listed in Table 2. The requirement that the PBH abundance is outside the regions constrained by observations dictates the choice of input parameters.

The critical collapse thresholds δ_c are calculated for each model using the procedure described in appendix A. The variations of input parameters and initial values in the ranges given in Table 2 do not substantially affect the shape of the spectra, so the variations of the corresponding critical collapse thresholds are insignificant. The obtained values are $\delta_c = 0.51$ for the PLLS model and $\delta_c = 0.56$ for the Tachyon model spectra. The fraction of PBH is calculated using Eqs. (102) and (108), with σ and μ obtained from (75) and (76), respectively. The data for the constraints are

Table 2: Input parameters corresponding to $f_{PBH}(M)$ plotted in Fig. 7

Model	$V_0[M_{Pl}^4]$	$\lambda \times 10^6$	$\phi_0[M_{Pl}]$	η_{in}	$\phi_{in}[M_{Pl}]$	δ_c	Line Style
PLLS $\alpha = 1.5$	10^{-16}	7.5490	0.835370	-1.4500×10^{-8}	5.2200	0.51	full
		7.5400	0.835370	-2.8174×10^{-7}	5.2500		dashed
		7.5400	0.835370	-2.8174×10^{-7}	5.3000		dash-dotted
		3.9523	0.895870	-1.0089×10^{-3}	5.1124		long dashed
Tachyon	10^{-16}	7.5020	0.259500	-6.1200×10^4	1.1000	0.56	full
					1.1005		dashed
					1.1010		dash-dotted
		7.6000	0.259831	-5.3625×10^4	1.0520		long dashed

Table 3: Integrated PBH DM fractions corresponding to $f_{PBH}(M)$ plotted in Fig. 7

Model	F_{PBH} [%]	Line Style
PLLS $\alpha = 1.5$	100	full blue
	9.0	dashed blue
	1.4	dash-dotted blue
	6.2	long dashed blue
Tachyon	10.6	full black
	5.3	dashed black
	2.6	dash-dotted black
	97.8	long dashed black

from Ref. [17].

The PLLS model with the set of parameters in Table 2 predicts the PBH fraction peaks in the observationally allowed windows of masses between 10^{-13} and 10^{-10} and between 10^{-6} and 10^{-4} solar masses. The Tachyon model, with the set of parameters in Table 2, predicts experimentally allowed PBH abundance today in a broad mass range from 10^{-16} to 10^6 solar masses, except for the special case (long dashed black line on Fig. 7) with the allowed masses between 10^{-14} and 10^{-10} solar masses.

For a DM prediction, we need the integrated PBH dark matter fraction. To this end, we use the definition (104) so the integrated PBH dark matter abundance in the mass interval (M_{min}, M_{max}) related to the total DM fraction is given by

$$F_{PBH} = \int_{M_{min}}^{M_{max}} f_{PBH} \frac{dM}{M}. \tag{109}$$

The results for both models are given in Table 3 for each set of parameters listed in Table 2. The PBH contribution to DM today could be significant and, in particular cases, even sufficient to account for the total DM. However, it is important to stress that the parameterization of the Tachyon model that leads to $F_{PBH} = 0.978$ corresponds to the spectrum not supported by the CMB observational data in the vicinity of the CMB pivot scale q_{CMB}.
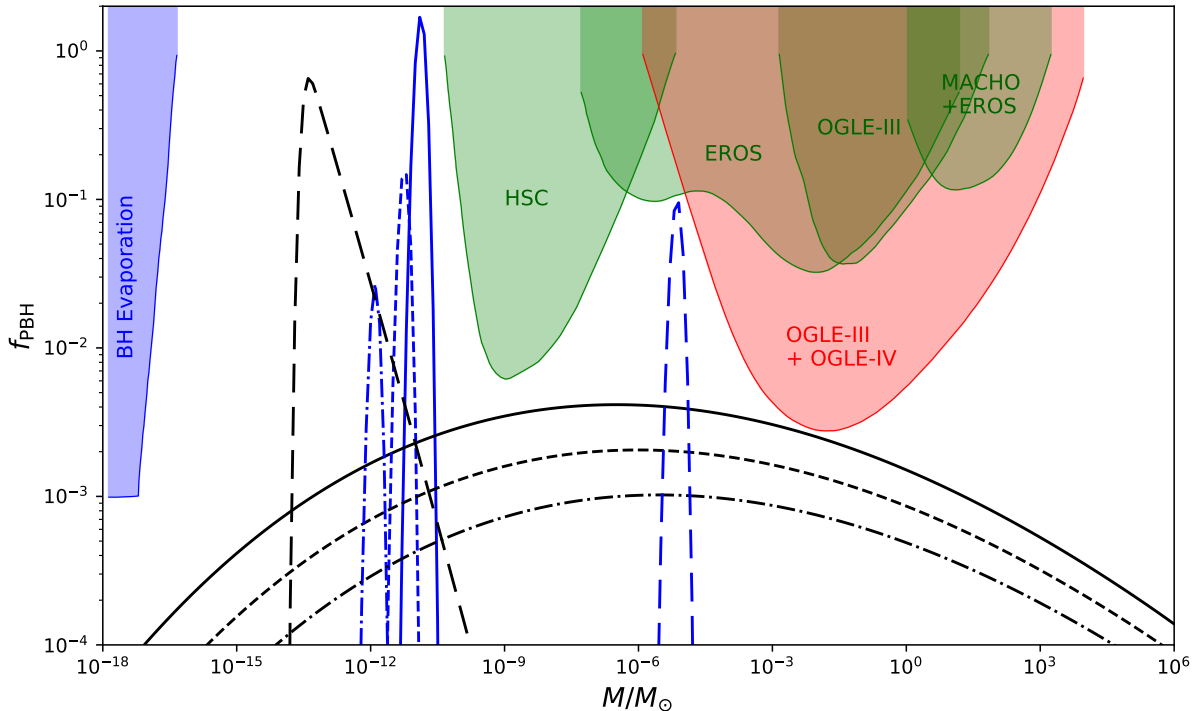
Figure 7: The fraction of PBH dark matter versus the PBH mass M in the PLLS model (blue lines) and the Tachyon model (black lines) together with observational constraints. The corresponding input parameters and initial values are listed in Table 2. The green contours mark the limits determined by EROS [12], OGLE-III [13], Hyper Suprime-Cam (HSC) [15], and MACHO+EROS [16]. The orange contour marks the constraints by OGLE-III + OGLE-IV [17].

5.2.1 Sensitivity to $\delta_{\rm c}$

The mass fraction β and consequently the PBH abundance calculated in both PS and CCP formalisms is exponentially sensitive to the critical collapse threshold $\delta_{\rm c}$. The value of δ_c depends on the shape of the collapsing curvature power spectrum [90] (see also [10, 77, 92, 83, 91, 93, 94, 95, 96]). In appendix A, we outline the calculation procedure. For a broad power spectrum that could be approximated by (78), we recover $\delta_c \sim 0.56$ of Ref. [90]. For the PLLS and Tachyon models, the variations of input parameters and initial values in the interesting ranges do not substantially affect the shape of the spectra. The variations of the corresponding critical collapse thresholds are within $\delta_{\rm c} = 0.51$ for the PLLS model and $\delta_{\rm c} = 0.56$ for the Tachyon model spectra.

In Fig. 8 we plot the mass fraction β and the PBH abundance $f_{\rm PBH}$ in the Tachyon model for various δ_c within the plausible uncertainty departure of about 1% from the numerical value calculated in appendix A.
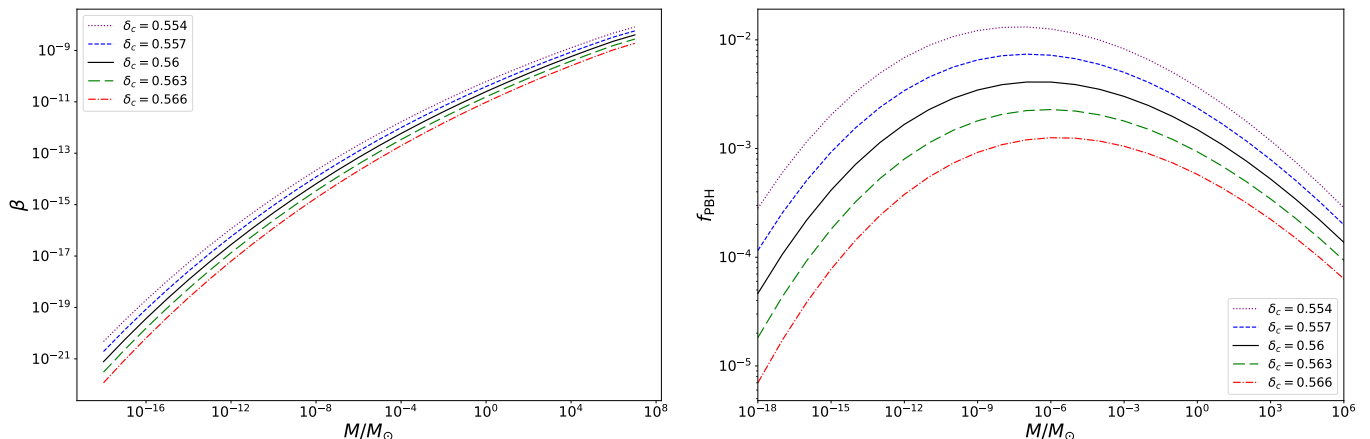
Figure 8: The mass fraction β (left panel) and fraction of PBH dark matter (right panel) versus M in the Tachyon model for various critical thresholds δ_{c} and fixed set of parameters as in Table 1 with $\phi_{\mathrm{in}} = 1.1 M_{\mathrm{Pl}}$.

5.3   Comment on primordial non-Gaussianity

The three-point correlation function

$$\langle \hat{\zeta}_{q_1} \hat{\zeta}_{q_2} \hat{\zeta}_{q_3} \rangle = (2\pi)^3 \delta(\boldsymbol{q}_1 + \boldsymbol{q}_2 + \boldsymbol{q}_3) f_{\mathrm{NL}} F(q_1, q_2, q_3) \tag{110}$$

provides the prime diagnostic of non-Gaussianity of inflationary fluctuations [97]. The quantity f_{NL} is a dimensionless parameter defining the amplitude of non-Gaussianity and the function F captures the momentum dependence.

The lowest-order non-Gaussian corrections to the primordial power spectrum arise from a single one-loop diagram, which leads to [98, 99, 100]

$$\mathcal{P}_{\mathrm{S}}(q) = \mathcal{P}_{\mathrm{S,G}}(q) + f_{\mathrm{NL}}^2 q^3 \int \frac{d^3 k}{4\pi} \frac{\mathcal{P}_{\mathrm{S,G}}(k)}{k^3} \frac{\mathcal{P}_{\mathrm{S,G}}(|\boldsymbol{q} - \boldsymbol{k}|)}{|\boldsymbol{q} - \boldsymbol{k}|^3}, \tag{111}$$

where $\mathcal{P}_{\mathrm{S,G}}$ is the dimensionless power spectrum defined in (50), and the second term on the right-hand side is a non-Gaussian contribution which can be rewritten as

$$\mathcal{P}_{\mathrm{S,NG}}(q) = f_{\mathrm{NL}}^2 q^2 \int_0^\infty \frac{dk}{k^2} \mathcal{P}_{\mathrm{S,G}}(k) \int_{|q-k|}^{q+k} \frac{dk'}{k'^2} \mathcal{P}_{\mathrm{S,G}}(k'). \tag{112}$$

Ünal [99] estimated (112) for the log-normal gaussian spectrum

$$\mathcal{P}_{\mathrm{S,G}} = A \exp[-\ln^2(k/k_{\mathrm{peak}})/(2\sigma^2)]. \tag{113}$$

For an amplitude $A = 0.01$, and $f_{\mathrm{NL}} = 3$, he found that the non-Gaussian term is subdominant by about a factor of 10. Clearly, if the amplitude were 10 times larger, the non-Gaussian term would be of the same order as the Gaussian one. Similarly, Riccardi, Taoso, and Urbano [101] found that in realistic single-field inflationary models with ultra slow-roll, by changing the peak amplitude of the curvature power spectrum by about a factor of two, one could obtain the same abundance calculated with the Gaussian approximation as the one obtained in the presence of local non-Gaussianities.

25

In the k-essence models, the largest non-Gaussianity peakes at the so-called *equilateral* configuration with $q_1 \sim q_2 \sim q_3$. The non-Gaussianity amplitude of an equilateral triangle in a general k-essence is given by [97, 102]

$$f_{\rm NL}^{\rm equil} = -\frac{35}{108}\left(\frac{1-c_{\rm s}^2}{c_{\rm s}^2}\right) + \frac{20}{81}\Lambda, \tag{114}$$

where

$$\Lambda \equiv X^2 \frac{\mathcal{L}_{XX}^2 - (1/3)\mathcal{L}_X \mathcal{L}_{XXX}}{\mathcal{L}_X^2 + 2X\mathcal{L}_X\mathcal{L}_{XX}}. \tag{115}$$

The quantity Λ in the Tachyon model is identically zero. As the sound speed deviates from unity most at the end of the slow roll regime, we estimate the equilateral amplitude at the end of inflation, neglecting possible post-inflationary effects. For an estimate we can use $c_{\rm s}^2 = 1/3$, given by (43) for $\varepsilon_1 = 1$, yielding

$$f_{\rm NL}^{\rm Tachyon} \approx f_{\rm NL}^{\rm equil}\Big|_{\varepsilon_1=1} = -\frac{70}{108}. \tag{116}$$

In the PLLS model, we find

$$\Lambda = \frac{1 - 3\alpha + 2\alpha^2}{3 + 6\alpha}, \tag{117}$$

so for $\alpha = 1.5$ we have $\Lambda = 1/12$. Thus, using (114) with $c_{\rm s}^2 = 1/2$, for the PLLS model we find $f_{\rm NL} \approx f_{\rm NL}^{\rm equil} = -295/972$

$$f_{\rm NL}^{\rm PLLS} \approx f_{\rm NL}^{\rm equil}\Big|_{\varepsilon_1=1} = -\frac{295}{972}. \tag{118}$$

Both values in (116) and (118) are well within the observational constraints provided by the Planck 2018 collaboration [103]: $f_{\rm NL}^{\rm equil} = -26 \pm 47$.

To estimate the NG contribution to the power spectrum in the PLLS model, we could approximate the spectrum of Fig. 4 by the log-normal function (113) with an amplitude of about $A = 0.1$. In our estimate, $f_{\rm NL} \simeq 0.3$, so the NG contribution to the power spectrum would amount to a factor of $(0.3/3)^2 = 0.01$ suppression compared to the NG term in Ref. [99]. Since our amplitude is a factor of 10 larger than that of Ref. [99], the NG contribution enhances the PLLS power spectrum of Fig. 4 by about 10%.

The results obtained for the log-normal spectrum of Ref. [99] cannot be used for the broad spectrum of our Tachyon model. However, we can obtain a rough estimate by making use of the top-hat power spectrum (78)). In this model, we find

$$\mathcal{P}_{\rm S,NG} = f_{\rm NL}^2 \mathcal{P}_0^2 q^2 \int_{q_{\rm min}}^{q_{\rm max}} \frac{dk}{k^2} \left[\frac{\Theta(|q-k|-q_{\rm min})\Theta(q_{\rm max}-|q-k|)}{|q-k|} \right.$$
$$\left. -\frac{\Theta(q+k-q_{\rm min})\Theta(q_{\rm max}-q-k)}{q+k}\right]. \tag{119}$$

The integration yields

$$\mathcal{P}_{\rm S,NG} = f_{\rm NL}^2 \mathcal{P}_0^2 \left[2\ln\frac{q^2 - q_{\rm min}^2}{q_{\rm min}^2} + 2\ln\frac{q_{\rm max}-q}{q_{\rm max}} - \frac{2q^2}{q^2 - q_{\rm min}^2} + \frac{q}{q_{\rm max}} + \frac{q}{q_{\rm max}-q}\right]. \tag{120}$$

In the middle of the distribution, where $q_{\rm min} \ll q \ll q_{\rm max}$ we find an estimate

$$\mathcal{P}_{\rm S,NG} \simeq 2f_{\rm NL}^2 \mathcal{P}_0^2 \left(\ln\frac{q^2}{q_{\rm min}^2} - 1 + \mathcal{O}(q_{\rm min}^2/q^2) + \mathcal{O}(q^2/q_{\rm max}^2)\right). \tag{121}$$

For our estimated $f_{\rm NL} \simeq -\frac{70}{108}$ and the parameters of our top-hat model of Fig. 6 $\mathcal{P}_0 = 0.09$, $q/q_{\min} = 10^4 \div 10^8$, we find $\mathcal{P}_{\rm S,NG} = 0.12 \div 0.24$, to be compared with $\mathcal{P}_{\rm S,G} = 0.09$. Hence, the NG contribution in the top-hat model is positive and of the order $\mathcal{O}(1 \div 2)\mathcal{P}_{\rm S,G}$. Thus, we expect the peak of the power spectrum that includes a non-Gaussian contribution in the Tachyon model to be enhanced by about a factor of $\mathcal{O}(2 \div 3)$ compared with the Gaussian power spectrum.

However, there is in addition an intrinsic non-Gaussianity owing to the nonlinear relation (70) between ζ and δ_r [81, 104, 105]. In the presence of such non-Gaussianity, the amplitude of the power spectrum can be significantly reduced by a factor $\mathcal{O}(2 \div 3)$ [105] compared to the Gaussian (linear) case, where one approximates (70) by the linear relation (71). In this way, the effect of this intrinsic non-Gaussianity works in the opposite direction compared to the primordial non-Gaussianity discussed above, so these two effects might partly annihilate. However, a precise estimate of the total outcome requires more accurate calculations, which go beyond the scope of the present paper.

Approximating the nonlinear relation (70) by the linear one can also affect the critical threshold $\delta_{\rm c}$. According to Kehagias, Musco, and Riotto [106], the impact of the intrinsic non-Gaussianity on a relative change of $\delta_{\rm c}$ with respect to the value obtained using a linear relation between ζ and δ_r is of the order of a few percent.

6   Summary and conclusions

We have analyzed the PBH production in the early universe in the top-hat toy model and two k-essence models of inflation. The analysis of the top-hat toy model reveals that the Press-Schechter prediction for the PBH mass fraction $f_{\rm PBH}$ based on Eq. (95) is by a factor of 100 larger than the prediction of the CCP formalism based on Eq. (102). For this reason, we have employed the more conservative CCP formalism in calculating $f_{\rm PBH}$ for realistic power spectra.

Besides, the analysis of the top-hat model shows that the PBH abundance is very sensitive to the height of the power spectrum. The top-hat power spectrum with height equal to or above 0.2 yields too large PBH abundance with $f_{\rm PBH} \gg 1$ whereas a height below 0.08 yields a small peak value of $f_{\rm PBH}$ less than 0.02.

Regarding the PLLS and Tachyon models, we have demonstrated that it is possible to obtain a significant PBH DM fraction by fine-tuning the input parameters, V_0, ϕ_0, λ, and initial conditions for the background equations. However, the normalization requirement for the spectrum to fit the observational value at the pivot CMB scale constrains the tuning of these parameters. This normalization requirement can be easily implemented by utilizing the rescaling invariance [57].

The PBH abundance is fairly sensitive to the value of the critical collapse threshold $\delta_{\rm c}$. We have found that the shape of the spectra in both models does not significantly change with slight variations in input parameters. As a consequence, the critical collapse threshold $\delta_{\rm c}$ is also not very sensitive to these variations. Hence, the values of $\delta_{\rm c}$ calculated for the spectra presented in Figs. 4 and 5 for the PLLS and the Tachyon model, respectively, could have been applied for each set of parameters presented in Table 2. However, as Fig. 8 shows, the relative change of $\delta_{\rm c}$ (e.g., caused by the intrinsic non-Gaussianity [106]) within about $\pm 1\%$ could affect the PBH production by a factor of up to $4 \div 6$.

Our results for the PLLS model show that a suitable choice of input parameters different from those in Ref. [31] could yield a significant PBH abundance. For a chosen set of parameters yielding the power spectrum of Fig. 4, the PBH fraction has a few sharp peaks around the PBH mass $M = 10^{-11} M_\odot$. In contrast, the Tachyon model power spectrum of Fig. 5 predicts experimentally allowed PBH abundance today in a broad mass range (Fig. 7). In the PLLS model, the integrated

PBH abundance of the highest peak (full blue line) in Fig. 7 could account for total DM. In the Tachyon model, the highest integrated contribution of PBHs to DM estimate is about 11% (full black line), except for a particular parameterization (long dashed black line) where the integrated PBH contribution may reach up to 98%. However, the latter result should not be taken seriously since the spectrum corresponding to this parameterization is not supported by the observational data near the CMB pivot scale.

A   The critical collapse threshold

The critical collapse threshold δ_c for PBH formation depends on the shape of the curvature perturbation spectrum. The shape parameter α describes the main features of the profile in the length-scale interval $0 < r < r_m$ where PBHs form. Here, we outline the procedure for calculating δ_c following Musco $et\ al.$ [90].

The first step is to compute the value of the comoving length scale $\hat{r}_m$ of the perturbation related to r_m via the coordinate transformation $r = \hat{r} \exp \zeta(\hat{r})$. To this end, we use the smoothed power spectrum $\mathcal{P}_S(q, \tau)$ defined as

$$\mathcal{P}_S(q, \tau) = \frac{2\pi^2}{q^3} \mathcal{P}_S(q) T^2(q\tau), \tag{122}$$

where the transfer function $T(x)$ is defined as

$$T(x) = 3 \frac{\sin(x/\sqrt{3}) - (x/\sqrt{3})\cos(x/\sqrt{3})}{(x/\sqrt{3})^3}. \tag{123}$$

The conformal time interval τ is, according to (61), approximately $\tau = -1/aH$. Now we assume that the scale $\hat{r}_m$ is a factor of 10 to 100 larger than the comoving horizon radius $1/(aH)$. Hence, in Eq. (123) we may substitute $-\hat{r}_m/p$ for τ, where p is a constant of order $10 \leq p \leq 100$ and, according to [90], the scale $\hat{r}_m$ is a positive root of the function

$$I(x) = \int_0^\infty \frac{dy}{y} \left[(y^2 - 1) \frac{\sin y}{y} + \cos y \right] \mathcal{P}_S(y/x) T^2(y/p). \tag{124}$$

As the next step, we compute the shape parameter α. First, we find the linear Gaussian shape parameter α_G using

$$\alpha_G = -\frac{1}{4} \left[1 + \frac{\int y\, dy \cos y\, \mathcal{P}_S(y/\hat{r}_m) T^2(y/p)}{\int dy \sin y\, \mathcal{P}_S(y/\hat{r}_m) T^2(y/p)} \right]. \tag{125}$$

Then, we compute the shape parameter α by solving the algebraic equation

$$F(\alpha)(1 + F(\alpha))\alpha = 2\alpha_G, \tag{126}$$

where

$$F(\alpha) = \left(1 - \frac{2}{5} \frac{e^{-1/\alpha} \alpha^{1-5/(2\alpha)}}{f(\alpha)} \right)^{1/2}, \tag{127}$$

with

$$f(\alpha) = \Gamma(5/(2\alpha)) - \Gamma(5/(2\alpha), 1/\alpha) \equiv \int_0^{1/\alpha} dt\, e^{-t} t^{5/(2\alpha)-1}. \tag{128}$$

Finally, we compute the threshold δ_c as a function of α. Up to a few percent precision, the threshold can be expressed as an analytic function

$$\delta_c(\alpha) = \frac{4}{15} \frac{e^{-1/\alpha} \alpha^{1-5/(2\alpha)}}{f(\alpha)}. \tag{129}$$

28

Acknowledgments

References

[1] Y. B. N. Zel'dovich I. D. Novikov, Soviet Astron. AJ, **10**, 602 (1967).

[2] S. Hawking, Mon. Not. Roy. Astron. Soc. **152**, 75 (1971).

[3] B. J. Carr and S. W. Hawking, Mon. Not. Roy. Astron. Soc. **168**, 399 (1974).

[4] B. J. Carr, Astrophys. J. **2**01, 1 (1975).

[5] G. F. Chapline, Nature **2**53.5489, 251 (1975).

[6] B. Carr and F. Kuhnel, Annual Review of Nuclear and Particle Science **70**, 355 (2020) [arXiv:2006.02838 [astro-ph.CO]].

[7] A. M. Green and B. J. Kavanagh, *Primordial Black Holes as a dark matter candidate, J. Phys. G* **48** (2021) 043001 [arXiv:2007.10722].

[8] I. Musco, Phys. Rev. D **100**, 123524 (2019) [arXiv:1809.02127 [gr-qc]].

[9] C. Germani and I. Musco, Phys. Rev. Lett. **122**, 141302 (2019) [arXiv:1805.04087 [astro-ph.CO]].

[10] A. Escrivà, C. Germani and R. K. Sheth, Phys. Rev. D **101**, 044022 (2020) [arXiv:1907.13311 [gr-qc]].

[11] B. Carr, K. Kohri, Y. Sendouda and J. Yokoyama, Rept. Prog. Phys. **84**, 116902 (2021) [arXiv:2002.12778 [astro-ph.CO]].

[12] P. Tisserand *et al.*, Astron. Astrophys. 469, 387–404 (2007).

[13] L. Wyrzykowski *et al.*, Mon. Not. R. Astron. Soc. 416, 2949–2961 (2011).

[14] K. M. Belotsky *et al.*, Mod. Phys. Lett. A **29**, 1440005 (2014) [arXiv:1410.0203 [astro-ph.CO]]; K. M. Belotsky *et al.*, Eur. Phys. J. C **79**, 246 (2019) [arXiv:1807.06590 [astro-ph.CO]].

[15] H. Niikura *et al.*, Nature Astronomy 3, 524–534 (2019).

[16] T. Blaineau *et al.*, Astron. Astrophys. 664, A106 (2022).

[17] P. Mróz *et al.*, Nature **632**, no.8026, 749-751 (2024) [arXiv:2403.02386 [astro-ph.GA]].

[18] B. J. Carr, J. H. Gilbert and J. E. Lidsey, Phys. Rev. D **50**, 4853-4867 (1994) [arXiv:astro-ph/9405027 [astro-ph]].

[19] M. Y. Khlopov, Res. Astron. Astrophys. **10**, 495-528 (2010) [arXiv:0801.0116 [astro-ph]]; M. Khlopov, Symmetry **16**, 1487 (2024).

[20] J. Garcia-Bellido and E. Ruiz Morales, Phys. Dark Univ. **18**, 47-54 (2017) [arXiv:1702.03901 [astro-ph.CO]].

[21] K. Kannike, L. Marzola, M. Raidal and H. Veermäe, JCAP **09**, 020 (2017) [arXiv:1705.06225 [astro-ph.CO]].

[22] C. Germani and T. Prokopec, Phys. Dark Univ. **18**, 6-10 (2017) [arXiv:1706.04226 [astro-ph.CO]].

[23] A. Y. Kamenshchik, A. Tronconi, T. Vardanyan and G. Venturi, Phys. Lett. B **791**, 201-205 (2019) [arXiv:1812.02547 [gr-qc]].

[24] G. Ballesteros and M. Taoso, Phys. Rev. D **97**, 023501 (2018) [arXiv:1709.05565 [hep-ph]].

[25] D. G. Figueroa, S. Raatikainen, S. Rasanen and E. Tomberg, Phys. Rev. Lett. **127**, no.10, 101302 (2021) [arXiv:2012.06551 [astro-ph.CO]].

[26] Y. F. Cai, X. Tong, D. G. Wang and S. F. Yan, Phys. Rev. Lett. **121**, no.8, 081306 (2018) doi:10.1103/PhysRevLett.121.081306 [arXiv:1805.03639 [astro-ph.CO]].

[27] C. Chen, X. H. Ma and Y. F. Cai, Phys. Rev. D **102**, no.6, 063526 (2020) [arXiv:2003.03821 [astro-ph.CO]].

[28] Y. Cai, M. Zhu and Y. S. Piao, Phys. Rev. Lett. **133**, no.2, 021001 (2024) [arXiv:2305.10933 [gr-qc]].

[29] S. W. Hawking, I. G. Moss and J. M. Stewart, Phys. Rev. D **26**, 2681 (1982)

[30] Z. Yi, Q. Gao, Y. Gong and Z. h. Zhu, Phys. Rev. D **103**, no.6, 063534 (2021) [arXiv:2011.10606 [astro-ph.CO]].

[31] T. Papanikolaou, A. Lymperis, S. Lola and E. N. Saridakis, JCAP **03** (2023), 003 [arXiv:2211.14900 [astro-ph.CO]].

[32] C. Armendariz-Picon, V. F. Mukhanov and P. J. Steinhardt, Phys. Rev. Lett. **85** (2000) 4438 [arXiv:astro-ph/0004134].

[33] C. Armendariz-Picon, T. Damour and V. F. Mukhanov, Phys. Lett. B **458** (1999) 209 [arXiv:hep-th/9904075].

[34] C. F. S. Pereira, D. C. Rodrigues, J. C. Fabris and M. E. Rodrigues, Phys. Rev. D **109**, 044011 (2024) [arXiv:2309.10963 [gr-qc]]; C. F. S. Pereira at al., Class. Quant. Grav. **42**, 015001 (2025) [arXiv:2405.07455 [gr-qc]]; C. F. S. Pereira *et al.*, Phys. Rev. D **111**, 084025 (2025) [arXiv:2409.09182 [gr-qc]]; C. F. S. Pereira *et al.*, Phys. Rev. D **111**, 124005 (2025) [arXiv:2503.09920 [gr-qc]].

[35] M. Fairbairn and M. H. G. Tytgat, Phys. Lett. B **546**, 1 (2002) [hep-th/0204070];

[36] A. V. Frolov, L. Kofman and A. A. Starobinsky, Phys. Lett. B **545**, 8 (2002) [hep-th/0204187];

[37] G. Shiu and I. Wasserman, Phys. Lett. B **541**, 6 (2002) [hep-th/0205003];

[38] M. Sami, P. Chingangbam and T. Qureshi, Phys. Rev. D **66**, 043530 (2002) [hep-th/0205179];

[39] G. Shiu, S. H. H. Tye and I. Wasserman, Phys. Rev. D **67**, 083517 (2003) [hep-th/0207119]; P. Chingangbam, S. Panda and A. Deshamukhya, JHEP **0502**, 052 (2005) [hep-th/0411210]; S. del Campo, R. Herrera and A. Toloza, Phys. Rev. D **79**, 083507 (2009) [arXiv:0904.1032]; S. Li and A. R. Liddle, JCAP **1403**, 044 (2014) [arXiv:1311.4664].

[40] L. Kofman and A. D. Linde, JHEP **0207**, 004 (2002) [hep-th/0205121].

[41] J. M. Cline, H. Firouzjahi and P. Martineau, JHEP **0211**, 041 (2002) [hep-th/0207156].

[42] F. Salamate, I. Khay, A. Safsafi, H. Chakir and M. Bennai, Mosc. Univ. Phys. Bull. **73** 405 (2018).

[43] N. Barbosa-Cendejas, R. Cartas-Fuentevilla, A. Herrera-Aguilar, R. R. Mora-Luna and R. da Rocha, JCAP. **2018** 005 (2018) [hep-th/1709.09016].

[44] D. M. Dantas, R. da Rocha and C. A. S. Almeida, Phys. Lett. B. **782** 149 (2018) [hep-th/1802.05638].

[45] D. A. Steer and F. Vernizzi, Phys. Rev. D **70**, 043527 (2004) [hep-th/0310139].

[46] N. Bilic, D. D. Dimitrijevic, G. S. Djordjevic, M. Milosevic and M. Stojanovic, JCAP **08**, 034 (2019) [arXiv:1809.07216 [gr-qc]].

[47] A. Y. Kamenshchik, A. Tronconi and G. Venturi, JCAP **01**, 051 (2022) [arXiv:2110.08112 [gr-qc]].

[48] B. Li, C. Chen and B. Wang, Phys. Lett. B **848**, 138365 (2024) [arXiv:2307.03747 [astro-ph.CO]].

[49] N. Bilić and G. B. Tupper, Central Eur. J. Phys. **12**, 147 (2014) [arXiv:1309.6588 [hep-th]].

[50] N. Bilić, S. Domazet and G. Djordjevic, Class. Quant. Grav. **34**, 165006 (2017) [arXiv:1704.01072 [gr-qc]].

[51] N. Bilic, D. Dimitrijevic, G. Djordjevic and M. Milosevic, Int. J. Mod. Phys. A **32**, 1750039 (2017) [arXiv:1607.04524 [gr-qc]].

[52] M. Stojanovic, N. Bilic, D. D. Dimitrijevic, G. S. Djordjevic and M. Milosevic, Int. J. Mod. Phys. A **38**, 2343003 (2023) [arXiv:2306.02423 [gr-qc]].

[53] G. W. Gibbons, Class. Quant. Grav. **20**, S321 (2003) [hep-th/0301117].

[54] A. Sen, JHEP **9910**, 008 (1999) [hep-th/9909062].

[55] M. Alishahiha, E. Silverstein and D. Tong, Phys. Rev. D **70**, 123505 (2004) [arXiv:hep-th/0404084 [hep-th]].

[56] S. E. Shandera and S.-H. H. Tye, JCAP **0605**, 007 (2006) [hep-th/0601099].

[57] N. Bilić, D. D. Dimitrijević, G. S. Djordjevic, M. Milošević and M. Stojanović, Universe **11**, 128 (2025) [arXiv:2502.06456 [gr-qc]].

[58] J. Garriga and V. F. Mukhanov, Phys. Lett. B **458**, 219-225 (1999) [arXiv:hep-th/9904176 [hep-th]].

[59] N. R. Bertini, N. Bilic and D. C. Rodrigues, Phys. Rev. D **102**, 123505 (2020) [erratum: Phys. Rev. D **105**, 129901 (2022)] [arXiv:2007.02332 [gr-qc]].

[60] V. F. Mukhanov, H. A. Feldman and R. H. Brandenberger, *Theory of cosmological perturbations. Part 1. Classical perturbations. Part 2. Quantum theory of perturbations. Part 3. Extensions*, Phys. Rept. **215**, 203 (1992).

[61] A. De and R. Mahbub, Phys. Rev. D **102**, 123509 (2020) [arXiv:2010.12685 [astro-ph.CO]].

[62] T. S. Bunch and P. C. W. Davies, Proc. Roy. Soc. Lond. A **360**, 117-134 (1978).

[63] D. Wands, K. A. Malik, D. H. Lyth and A. R. Liddle, Phys. Rev. D **62**, 043527 (2000) [arXiv:astro-ph/0003278 [astro-ph]].

[64] S. Young and M. Musso, JCAP **11**, 022 (2020) [arXiv:2001.06469 [astro-ph.CO]].

[65] S. Young, "Computation of the Abundance of Primordial Black Holes," [arXiv:2405.13259 [astro-ph.CO]].

[66] A. M. Green and A. R. Liddle, Phys. Rev. D **56**, 6166-6174 (1997) [arXiv:astro-ph/9704251 [astro-ph]].

[67] R. Scoccimarro, Astrophys. J. **487**, 1 (1997) [arXiv:astro-ph/9612207 [astro-ph]].

[68] A. M. Green, A. R. Liddle, K. A. Malik and M. Sasaki, Phys. Rev. D **70**, 041502 (2004) [arXiv:astro-ph/0403181 [astro-ph]].

[69] T. Bringmann, C. Kiefer and D. Polarski, Phys. Rev. D **65**, 024008 (2002) doi:10.1103/PhysRevD.65.024008 [arXiv:astro-ph/0109404 [astro-ph]].

[70] D. Blais, T. Bringmann, C. Kiefer and D. Polarski, Phys. Rev. D **67**, 024024 (2003) [arXiv:astro-ph/0206262 [astro-ph]].

[71] K. Ando, K. Inomata and M. Kawasaki, Phys. Rev. D **97**, no.10, 103528 (2018) [arXiv:1802.06393 [astro-ph.CO]].

[72] K. Ando, M. Kawasaki and H. Nakatsuka, Phys. Rev. D **98**, no.8, 083508 (2018) [arXiv:1805.07757 [astro-ph.CO]].

[73] S. Young, Int. J. Mod. Phys. D **29**, no.02, 2030002 (2019) [arXiv:1905.01230 [astro-ph.CO]].

[74] V. De Luca, G. Franciolini and A. Riotto, Phys. Lett. B **807**, 135550 (2020) [arXiv:2001.04371 [astro-ph.CO]].

[75] E. W. Kolb and M. S. Turner, The Early Universe, Addison and Wesley, vol. 69. 1990, 10.1201/9780429492860.

[76] M. Sasaki, T. Suyama, T. Tanaka and S. Yokoyama, Class. Quant. Grav. **35**, 063001 (2018) [arXiv:1801.05235 [astro-ph.CO]].

[77] N. Bhaumik and R. K. Jain, JCAP **01**, 037 (2020) [arXiv:1907.04125 [astro-ph.CO]]

[78] Yogesh and A. Mohammadi, Astrophys. J. **986**, 35 (2025) [arXiv:2501.01867 [gr-qc]].

[79] https://mathworld.wolfram.com/Erfc.html

[80] J. C. Niemeyer and K. Jedamzik, Phys. Rev. Lett. **80**, 5481-5484 (1998) [arXiv:astro-ph/9709072 [astro-ph]].

[81] S. Young, I. Musco and C. T. Byrnes, JCAP **11**, 012 (2019) [arXiv:1904.00984 [astro-ph.CO]].

[82] T. Koike, T. Hara and S. Adachi, Phys. Rev. Lett. **74**, 5170-5173 (1995) [arXiv:gr-qc/9503007 [gr-qc]].

[83] P. S. Cole and J. Fumagalli, Universe **11**, no.9, 322 (2025) [arXiv:2509.14326 [astro-ph.CO]].

[84] N. Kitajima, Y. Tada, S. Yokoyama and C. M. Yoo, JCAP **10**, 053 (2021) [arXiv:2109.00791 [astro-ph.CO]].

[85] C. M. Yoo, T. Harada, S. Hirano and K. Kohri, PTEP **2021**, no.1, 013E02 (2021) [erratum: PTEP **2024**, no.4, 049203 (2024)] doi:10.1093/ptep/ptaa155 [arXiv:2008.02425 [astro-ph.CO]].

[86] S. Pi, M. Sasaki, V. Takhistov and J. Wang, JCAP **09**, 045 (2025) [arXiv:2501.00295 [astro-ph.CO]].

[87] K. Inomata, M. Kawasaki, K. Mukaida, Y. Tada and T. T. Yanagida, Phys. Rev. D **96**, 043504 (2017) [arXiv:1701.02544 [astro-ph.CO]].

[88] C. T. Byrnes, M. Hindmarsh, S. Young and M. R. S. Hawkins, JCAP **08**, 041 (2018) [arXiv:1801.06138 [astro-ph.CO]].

[89] S. Pi, Y. l. Zhang, Q. G. Huang and M. Sasaki, JCAP **05**, 042 (2018), [arXiv:1712.09896 [astro-ph.CO]].

[90] I. Musco, V. De Luca, G. Franciolini and A. Riotto, Phys. Rev. D **103**, 063538 (2021) [arXiv:2011.03014 [astro-ph.CO]].

[91] T. Harada, C. M. Yoo and K. Kohri, Phys. Rev. D **88**, no.8, 084051 (2013) [erratum: Phys. Rev. D **89**, no.2, 029903 (2014)] [arXiv:1309.4201 [astro-ph.CO]].

[92] I. Dalianis, A. Kehagias and G. Tringas, JCAP **01**, 037 (2019) [arXiv:1805.09483 [astro-ph.CO]].

[93] I. Musco, J. C. Miller and L. Rezzolla, Class. Quant. Grav. **22**, 1405-1424 (2005) [arXiv:gr-qc/0412063 [gr-qc]].

[94] A. Kalaja, N. Bellomo, N. Bartolo, D. Bertacca, S. Matarrese, I. Musco, A. Raccanelli and L. Verde, JCAP **10**, 031 (2019) [arXiv:1908.03596 [astro-ph.CO]].

[95] A. Escrivà and A. E. Romano, JCAP **05**, 066 (2021) [arXiv:2103.03867 [gr-qc]].

[96] I. D. Stamou, Phys. Rev. D **108**, no.6, 063515 (2023) [arXiv:2306.02758 [astro-ph.CO]].

[97] D. Baumann, *Inflation*, in Proceedings of TASI09, Physics of the Large and the Small, pp. 523-686 (2011). [arXiv:0907.5424 [hep-th]].

[98] [C. T. Byrnes, K. Koyama, M. Sasaki and D. Wands, JCAP **11**, 027 (2007) [arXiv:0705.4096 [hep-th]]

[99] C. Ünal, Phys. Rev. D **99**, no.4, 041301 (2019) [arXiv:1811.09151 [astro-ph.CO]];

[100] Z. H. Wang, H. L. Huang and Y. S. Piao, Phys. Rev. D **111**, no.8, 083553 (2025) [arXiv:2501.08542 [astro-ph.CO]].

[101] M. Taoso and A. Urbano, JCAP **08**, 016 (2021) [arXiv:2102.03610 [astro-ph.CO]]; F. Riccardi, M. Taoso and A. Urbano, JCAP **08**, 060 (2021) [arXiv:2102.04084 [astro-ph.CO]].

[102] X. Chen, M. x. Huang, S. Kachru and G. Shiu, *Observational signatures and non-Gaussianities of general single field inflation*, JCAP **0701**, 002 (2007) [hep-th/0605045].

[103] Y. Akrami *et al.* [Planck], "Planck 2018 results. IX. Constraints on primordial non-Gaussianity," Astron. Astrophys. **641**, A9 (2020) [arXiv:1905.05697 [astro-ph.CO]].

[104] M. Kawasaki and H. Nakatsuka, Phys. Rev. D **99**, no.12, 123501 (2019) [arXiv:1903.02994 [astro-ph.CO]].

[105] V. De Luca, G. Franciolini, A. Kehagias, M. Peloso, A. Riotto and C. Ünal, JCAP **07**, 048 (2019) [arXiv:1904.00970 [astro-ph.CO]].

[106] A. Kehagias, I. Musco and A. Riotto, JCAP **12**, 029 (2019) [arXiv:1906.07135 [astro-ph.CO]].